New insights on the interseismic active deformation along the North Ecuadorian–South Colombian (NESC) margin

Kevin Manchuel,[1] Marc Régnier,[2] Nicole Béthoux,[1] Yvonne Font,[3] Valentí Sallarès,[4] Jordi Díaz,[5] and Hugo Yepes[6]

Received 7 July 2010; revised 29 January 2011; accepted 12 April 2011; published 21 July 2011.

[1] The North Ecuadorian–South Colombian subduction zone was the site of the 1906 Mw 8.8 megathrust earthquake. This main shock was followed by three large events in 1942, 1958, and 1979 whose rupture zones were located within the 500 km long 1906 rupture area. A combined onshore and offshore temporary seismic network covering from the trench to the Andes was deployed during 3 months in the area of large earthquakes, in order to obtain a detailed knowledge of the seismic background activity. Resulting earthquakes location and mechanisms bring new insights on interseismic active deformation distribution in the three main tectonic units of the margin, namely, the Interplate Seismogenic Zone, the fore-arc region which is part of the North Andean Block and the downgoing oceanic Nazca plate. The interplate seismic activity presents along strike variations, suggesting that the seismicity and the associated stress buildup along the plate interface depend on the time elapsed since the last large earthquakes. According to our results, the updip and downdip limits of the seismogenic zone appear to be located at 12 and 30 km depth, respectively. Shallow to intermediate depth seismicity indicates a slab dip angle of ≈25°. North of the Carnegie Ridge, the Wadati-Benioff plane is defined beneath the fore arc down to ≈100 km depth. Facing the ridge, the Wadati-Benioff plane extends beneath the Andes, down to ≈140 km depth. This observation conflicts with the hypothesis of the presence of a flat slab at a depth of 100 km facing the ridge. In the overlying fore-arc region, the crustal seismicity occurs down to 40 km depth and is mainly concentrated in a roughly NW-SE 100 km wide stripe stretching from the coast, at about 1°N, to the Andes. The location of this active deformation stripe coincides with observed tectonic segmentation of the coastal domain as evidenced by the presence of an uplifting segment to the south and a subsiding segment to the north of the stripe. It also corresponds to a ≈30° change in the trend of the Andes, suggesting that the curvature of the volcanic arc might play an important role in the deformation of the fore-arc region.

Citation: Manchuel, K., M. Régnier, N. Béthoux, Y. Font, V. Sallares, J. Díaz, and H. Yepes (2011), New insights on the interseismic active deformation along the North Ecuadorian–South Colombian (NESC) margin, *Tectonics*, *30*, TC4003, doi:10.1029/2010TC002757.

1. Introduction

[2] In subduction zones, the seismic cycle consists of three main phases [*Reid*, 1910; *Stein and Ekstrom*, 1992]: (1) an interseismic period during which stress is accumulated over a relatively long period along the interplate seismogenic zone (ISZ), (2) the coseismic phase during which the accumulated stress is suddenly released through large megathrust earthquakes, and (3) the postseismic phase, corresponding to the total stress relaxation along the plate interface, which is characterized by the occurrence of aftershocks. Some authors have proposed that the seismic cycle is accompanied by characteristic patterns in seismicity, with alternation, in space and time, of periods of quiescence and of intensive seismicity along the plate interface [*Fedotov*, 1965; *Mogi*, 1977, 1985; *Scholz*, 1988, 1990]. This seismicity distribution correlates with surface rupture and asperity spatial determination, and would be related to stress buildup along the plate interface [*Bollinger et al.*, 2004].

[3] Along the North Ecuadorian–South Colombian (NESC) subduction zone, four megathrust earthquakes have occurred

[1]UMR Geoazur, University of Nice–Sophia Antipolis, Villefranche-sur-Mer, France.
[2]UMR Geoazur, University of Nice–Sophia Antipolis, IRD, Sophia-Antipolis, Valbonne, France.
[3]UMR Geoazur, University of Nice–Sophia Antipolis, IRD, Villefranche-sur-Mer, France.
[4]Unidad de Tecnología Marina, Consejo Superior de Investigaciones Científicas, Passeig Maritim de la Barceloneta, Barcelona, Spain.
[5]Departamento Geofisica i Tectonica, Institut de Ciències de la Terra "Jaume Almera" IJA-CSIC, Barcelona, Spain.
[6]Instituto Geofisico de la Escuela Politecnica Nacional, Quito, Ecuador.

0278-7407/11/2010TC002757

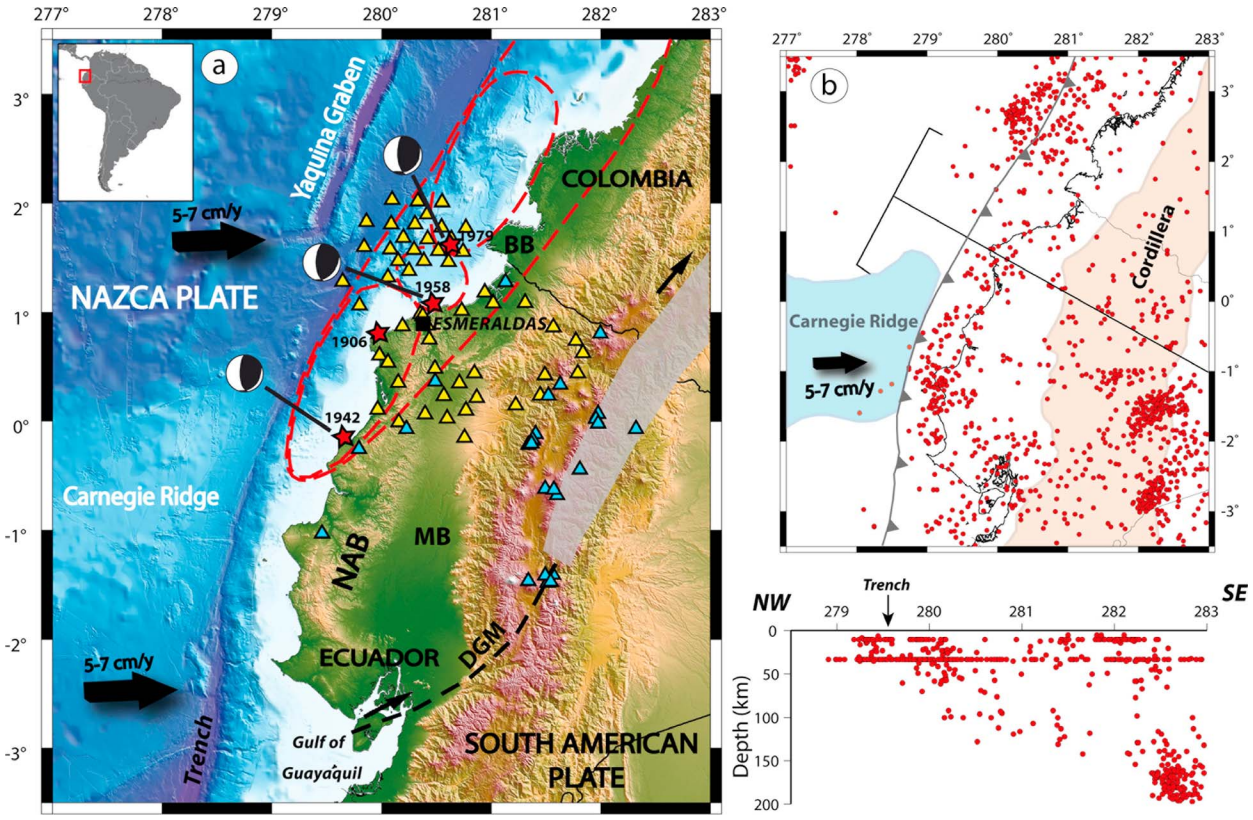

Figure 1. (a) Geodynamic setting of the North Ecuadorian–South Colombian active margin. Bathymetry compilation is from *Michaud et al.* [2006]. Nazca plate motion vectors are from *Trenkamp et al.* [2002]. Red dashed lines represent the surface rupture of the four great subduction earthquakes that occurred during the twentieth century, and red stars represent their epicenters [from *Mendoza and Dewey*, 1984]. Associated focal mechanisms are lower hemisphere projection. Triangles represent the locations of the seismological stations used in this study (yellow triangles are for the ESMERALDAS networks stations, and blue ones are for the Instituto Geofísico de la Escuela Politécnica Nacional permanent network, RENSIG). DGM = Dolores Guayaquil Megashear (gray area represents portion of the fault system still debated), MB = Manabí Basin, BB = Borbón Basin, and NAB = North Andean Block. (b) NEIC seismicity along the NESC active margin both on map and cross section. Black line on the map represents the cross section location and width.

during the twentieth century (Figure 1 and Table 1). The 500 km long rupture zone of the larger event (Mw = 8.8), which occurred in 1906 [*Kelleher*, 1972; *Kanamori and Given*, 1981; *Kanamori and McNally*, 1982] was partially reactivated by the ruptures of three smaller thrust events [*Mendoza and Dewey*, 1984] in 1942 (Mw = 7.8) [*Swenson and Beck*, 1996], 1958 (Mw = 7.7) and 1979 (Mw = 8.2) [*Herd et al.*, 1981; *Kanamori and McNally*, 1982; *Beck and Ruff*, 1984] (Figure 1). There is a shortage of energy between that released during the largest 1906 earthquake and the cumulative coseismic energy of the other three more recent ones (Table 1). Concerning the seismological asperities, as evidenced by high quality MCS seismic lines for the 1979 asperity, these areas of maximum slip likely correspond to structural heterogeneities [*Collot et al.*, 2002]. The spatial and chronological organization of these megathrust earthquakes, together with their associated seismic moments (Table 1), suggests that two seismic cycles may be nested in the study area. Based on the recurrence time between large earthquakes and on the estimates of coseismic displacements,

Table 1. Main Characteristics of the 1906, 1942, 1958, and 1979 Large Earthquakes[a]

Date	Latitude	Longitude	Magnitude (Mw)	Depth (km)	Surface Rupture Length	Seismic Moment (10^{24} dyne cm)
31/01/1906	1°N	81.5°W	8.8 (2)	?	500 (1)	200 (2)
14/05/1942	0.01°N	80.39°W	7.8	19.7; 14 (4)	200 (4)	3.2 (2)
19/01/1958	1.14°N	79.59°W	7.7	29.8; 18.5 (5)	50 (3)	5.2 (2)
12/12/1979	1.62°N	79.42°W	8.2	37.5; 24.3 (5)	170–240 (3)	29 (2)

[a]The 1906 earthquake location is from *Gutenberg and Richter* [1959] and the 1942, 1958, and 1979 earthquake locations are from *Mendoza and Dewey* [1984]. Numbers in parentheses are as follows: 1, *Kelleher* [1972]; 2, *Kanamori and McNally* [1982]; 3, *Beck and Ruff* [1984]; 4, *Swenson and Beck* [1996]; 5, *Engdahl and Villaseñor* [2002].

Nishenko [1991] pointed out that the NESC margin presents one of the highest seismic hazards of South America.

[4] All the epicenters of the twentieth century large interplate earthquakes were located north of the Carnegie Ridge (Figure 1), a ≈200 km wide buoyant volcanic and aseismic ridge [*Lonsdale*, 1978] that forms a structural high in the downgoing oceanic Nazca plate. The southward extension of their rupture areas stoped on the northern flank of the ridge (Figure 1). Facing the ridge and south of it, the instrumental seismicity shows a radically different pattern, without known historical earthquakes except the Mw = 7.1 earthquake of Bahia de Caraquez in 1998 [*Segovia*, 2001]. In this area, the seismicity is mainly organized in interplate swarms, occurring during seismic crisis such as the Manta crisis in 2005 [*Vaca et al.*, 2009]. The interplate seismic activity along the Ecuadorian margin indicates a seismological segmentation that seems to be related with the subduction of the Carnegie Ridge.

[5] The spatiotemporal distribution of the background seismicity in the fore-arc region is poorly constrained. Global catalogs, such as NEIC, provide a diffuse image of the Ecuadorian seismicity (Figure 1b). The *Instituto Geofisico de la Escuela Politecnica Nacional* runs the National Ecuadorian Seismic Network (RENSIG). These stations are mainly deployed in the Andes in order to monitor volcanic hazards. Consequently, the investigation of coastal seismic events suffers from a poor azimuthal coverage. Two local seismological studies have been carried out in the region to study specific active tectonic targets. The LITHOSCOPE (1995) temporary network was mainly deployed around the Cordillera, to determine active deformation beneath the Ecuadorian Andes [*Guillier et al.*, 1996; *Guillier et al.*, 2001]. In 1998, an offshore OBS network was deployed during the SUBLIME experiment to characterize seismicity from the trench to the coast [*Pontoise and Monfret*, 2004]. Finally, we carried out the ESMERALDAS experiment in 2005, in order to better resolve active structures involved in the large earthquakes area, covering the region from the trench to the Cordillera.

[6] The ESMERALDAS experiment consisted in the deployment of a combined offshore-onshore temporary network. The large coverage and increased station density achieved by the ESMERALDAS network, aimed at better sampling the microseismicity (M < 5), refining seismic events location and consequently improving the knowledge on active deformation across the fore-arc region. This paper deals with the analysis of the recorded seismic data together with the information available from global and regional catalogs. Accurate seismicity distribution brings new constraints on the interplate seismic activity related to the twentieth century megathrust earthquakes sequence. We also characterize the geometry and the mode of deformation of the three main tectonic units of the margin: ISZ, upper plate and subducting oceanic Nazca plate.

2. Geodynamical, Seismological and Geological Setting

[7] The <25 My old oceanic Nazca plate [*Hardy*, 1991] is subducting beneath Ecuador at a rate of approximately 5–7 cm/yr in a roughly east-west direction [*Trenkamp et al.*, 2002; *Nocquet et al.*, 2009; *Kendrick et al.*, 2003]. South of 0.5°N the trench is oriented north-south, while north of it its azimuth changes to a northeast direction and the convergence therefore becomes oblique (Figure 1). This obliquity is accommodated along the Dolores-Guayaquil Megashear (Figure 1), by the long-term northeastward motion of the North Andean Block (NAB) with respect to the South American plate, at a rate of 7–10 mm/yr (Figure 1) [*Kellogg and Vega*, 1995; *Ego et al.*, 1996]. The boundary between the NAB and the South American plate is still debated, in particular between 1°S and 1°N (Figure 1). The NAB displacement is accompanied by the opening of the Gulf of Guayaquil and the formation of quaternary NW-SE normal faulting in the fore-arc region [*Daly*, 1989; *Benítez*, 1995; *Deniaud*, 2000; *Dumont et al.*, 2005; *Witt et al.*, 2006; *Witt and Bourgois*, 2010]. The NAB consists of several mafic to ultramafic oceanic terranes accreted since the Mesozoic to the South American Plate [*Jaillard et al.*, 1997; *Reynaud et al.*, 1999; *Cediel et al.*, 2003; *Luzieux et al.*, 2006; *Collot et al.*, 2008].

[8] The ESMERALDAS network covers two tectonic segments of the upper plate. South of Esmeraldas city, facing the Carnegie Ridge, the margin is uplifted [*Dumont et al.*, 2005; *Pedoja et al.*, 2006a, 2006b], while north of it subsidence has prevailed during the Quaternary [*Deniaud*, 2000]. It has been suggested that the Carnegie Ridge is responsible for the uplift of the central part of the Ecuadorian coast [*Daly*, 1989; *Gutscher et al.*, 1999]. The age of initiation of the Carnegie Ridge subduction is still debated, and may have begun between the late Miocene [*Daly*, 1989; *Gutscher et al.*, 1999] and the late Pliocene–Upper Pleistocene [*Lonsdale*, 1978; *Sallarès and Charvis*, 2003; *Pedoja et al.*, 2006a, 2006b; *Michaud et al.*, 2009].

[9] The age of the initiation of the Carnegie Ridge subduction is a key to determine the subducted ridge length and consequently its possible influence on the slab geometry. Based on the analysis of the International Seismological Centre (ISC) catalog, *Gutscher et al.* [1999] proposed the presence of a flat slab at ≈0°N. They suggest that the flattening of the slab would be a consequence of the extra buoyancy of the Carnegie Ridge. This interpretation contrasts with the 35° dipping slab proposed further north by *Guillier et al.* [2001] based on the local events reported at several seismological catalogs. *Pontoise and Monfret* [2004], using the RENSIG catalog to complete their results also suggested that the Wadati-Benioff plane dips roughly with an angle of about 35° beneath the fore arc and the Andes.

[10] NESC crustal structures between the trench and the coast have been recognized from several geophysical marine experiments. Available wide-angle seismic data provide good constraints on the crustal thickness and velocity structure on the frontal part of the subduction system offshore Ecuador [*Sallarès and Charvis*, 2003; *Calahorrano et al.*, 2004, 2008; *Graindorge et al.*, 2004; *Sallarès et al.*, 2005; *Gailler et al.*, 2007; *Garcia Cano*, 2009]. MCS data acquired in the area during the SISTEUR project in 2000, show the presence of structural heterogeneities both in the Nazca plate and the NAB. *Collot et al.* [2004] suggested that these features may limit the rupture zones of the great NESC margin earthquakes. In addition, coincident wide-angle seismic profiles, perpendicular to the trench, indicate that the dip angle of the interplate boundary is about 10° at the frontal part of the subduction [*d'Acremont et al.*, 2005; *Gailler et al.*, 2007; *Collot et al.*, 2008; *Agudelo*, 2005; *Agudelo et al.*, 2009]. This dip angle is in agreement with that estimated by *Pontoise and Monfret* [2004] in the ISZ, based on the

Table 2a. P Velocity Model Used at Ocean Bottom Seismometers for Hypocenter Inversion [From *Agudelo*, 2005; *Agudelo et al.*, 2009; *Gailler et al.*, 2007; *Collot et al.*, 2008][a]

Z (km)	Vp
0.0	2.8
3.0	5.0
8.0	6.3
17.0	8.15

[a]The Vs model is obtained using Vp/Vs ratio of 1.78.

SUBLIME event locations. These authors suggested that the updip limit of the ISZ is recognized at 12 km depth [*Pontoise and Monfret*, 2004], and it has been correlated to a low thermal value of 60–70°C [*Marcaillou et al.*, 2008].

[11] The ESMERALDAS temporary seismic network used in this experiment spreads over a region were both tectonical and seismological changes occur. Our study provides new constraints on seismicity distribution and active deformation along the highly segmented NESC margin.

3. Seismological Data and Data Processing

3.1. Network Configuration

[12] The ESMERALDAS passive experiment was carried out from March 10 to June 14, 2005. Twenty-six Ocean Bottom Seismometers (OBS) and 31 seismic land stations were deployed during this experiment (Figure 1). Nine of the OBS were equipped with Guralp GMG40T 3C broadband marine sensors [*Hello et al.*, 2006], and the rest with short period seismometers (4.5 Hz). Land stations included broad band sensors (2 CMG-3T and 4 CMG-40T from Guralp), intermediate-period sensors (8 Lennartz-20s, 14 Lennartz-5s) and short period sensors (3 Mark Products L4C-1s). In order to reduce the azimuthal gap, we also included records from available RENSIG stations (Figure 1).

3.2. Location Technique

[13] P and S picks and preliminary locations were performed with the SEISAN code [*Havskov and Ottemöller*, 1999]. Given the crustal structure variations from the outer trench to the volcanic arc, we used different reference velocity models depending on the station location. Final hypocenter locations were computed using HYPOELLIPSE code [*Lahr*, 1999], and applying different 1D velocity models for the different stations. For OBS, the P wave velocity model (Table 2a) was derived from a wide-angle seismic model in the network area [*Agudelo*, 2005; *Agudelo et al.*, 2009; *Gailler et al.*, 2007; *Collot et al.*, 2008]. A single seismic refraction profile acquired in the high Andes during the Project Nariño [*Ocola et al.*, 1975], provides the only available crustal velocity information relevant for the Ecuadorian fore-arc domain. To better constrain earthquakes location by accounting for the east-west upper crustal thickness variations, we initially used two velocity models for the stations located on the upper plate (the CRUST2.0 [*Bassin et al.*, 2000] velocity model for the stations located from the coast to the Cordillera and the Project Nariño velocity model [*Ocola et al.*, 1975] for the stations located on the volcanic arc). Event location results were not significantly improved compared to those obtained with the use of the single CRUST2.0 [*Bassin et al.*, 2000] velocity model (Table 2b) for all NAB stations. Consequently, the final locations displayed in Figure 2 were calculated using a unique velocity model for the land stations, which corresponds to the CRUST2.0, a global earth velocity model specified from 2*2 degree [*Bassin et al.*, 2000]. From OBS data, we computed a Vp/Vs ratio of 1.78 (Table 2a), using a linear correlation between P and S arrival times [*Wadati*, 1933]. *Pontoise and Monfret* [2004] determined a Vp/Vs ratio of 1.81 from the data of the SUBLIME experiment (1998), with OBS located just south of the ESMERALDAS network. This Vp/Vs discrepancy may be linked to uncertainties in OBS S wave arrival time measurement and/or lateral heterogeneities of the margin. For land stations we obtained a Vp/Vs ratio of 1.74 (Table 2b). This value is better constrained than offshore thanks to the larger number of clearer seismic phases identified, especially S wave arrivals.

[14] From the ESMERALDAS records, 544 events were detected and extracted from continuous data, among which 368 events have travel time RMS value smaller than 1.5 s. 263 events exhibit A, B, or C quality, according to HYPOELLIPSE criteria [*Lahr*, 1999] (Figure 2). As conventionally assumed, quality A, B and C are associated to the values of SEH (the horizontal 68% confidence limit in the least well-constrained direction) and SEZ (the 68% confidence limit for depth). Quality A, B and C correspond to SEH and SEZ smaller than 1.34 km, 2.67 km and 5.35 km, respectively [*Lahr*, 1999]. In Figure 3a we show a histogram of the RMS normalized by the number of phases used for the location, taking into account the different class of quality. These ranges of small errors are statistical and generally underestimated. They do not warrant an absolute value of the focal locations uncertainties. Nevertheless, they certify the coherence on location accuracy with 59% of A quality location (among A, B and C quality). The location of the network, just above the seismicity and surrounding the epicenters also provides a good confidence in the locations [*Bondár et al.*, 2004].

3.3. Magnitude Determination

[15] 214 events are included in both ESMERALDAS and RENSIG catalogs. We used the RENSIG duration magnitude (Md), derived using Mb magnitude from global catalogs, to build a local magnitude law based on the maximum amplitude measurement read on ESMERALDAS seismograms. First, we measured the maximum amplitude $A(i,j)$ for an event i (included in the 214 common events) at the j ESMERALDAS station. The RENSIG magnitudes are then expanded as

$$M_{rensig}(i) = \alpha \log[A(i,j)] + \beta \log[D(i,j)] + C_j$$

Table 2b. P Velocity Model Used at Land Stations for Hypocenter Inversion [From *Bassin et al.*, 2000][a]

Z (km)	Vp
0.0	2.5
0.5	4.0
1.0	6.0
11.0	6.6
22.0	7.2
32.0	8.15

[a]The Vs model is obtained using Vp/Vs ratio of 1.74.

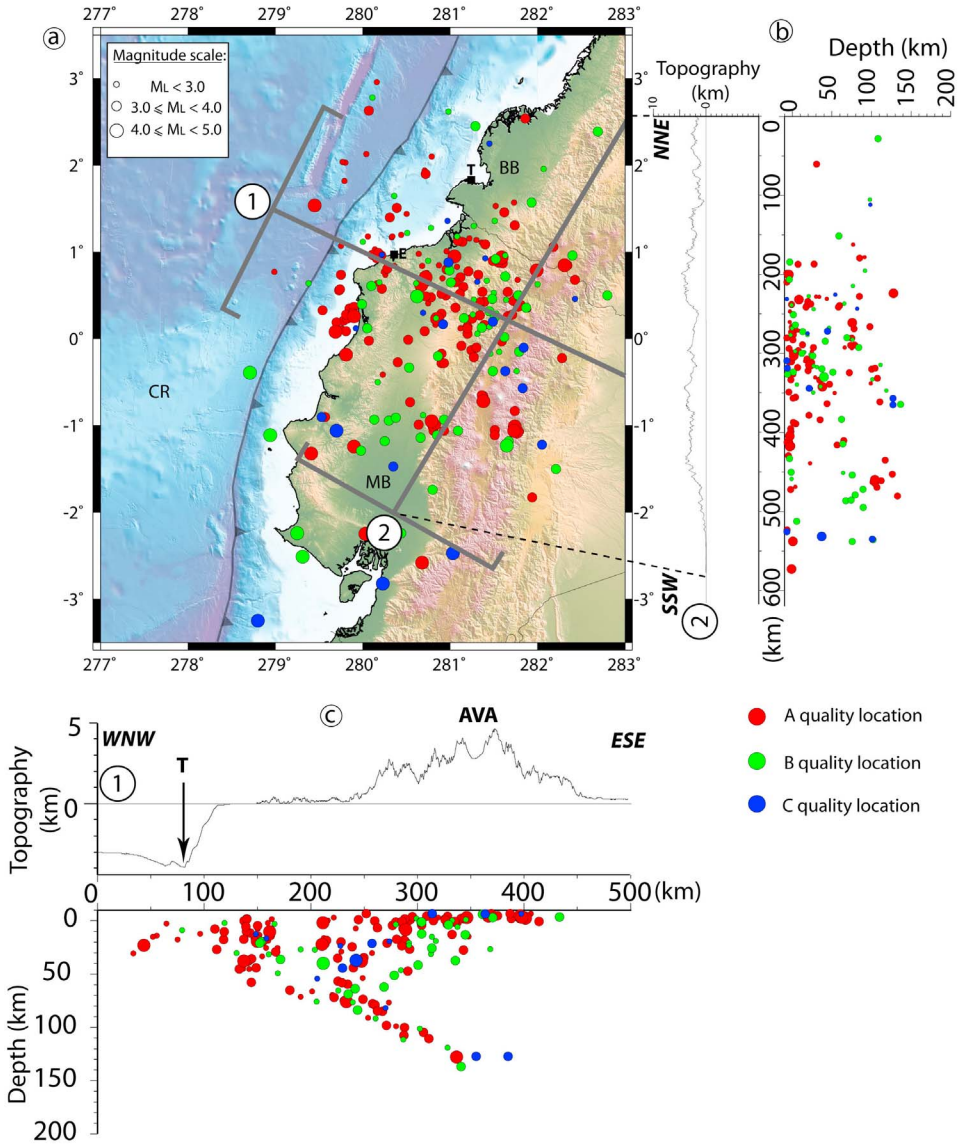

Figure 2. (a) Events location and magnitude resulting from the ESMERALDAS experiment. Location and width of the cross sections are represented on the map by gray lines. Circle colors correspond to location quality according to the HYPOELLIPSE criteria (see text for reference and quality determination explanation); size represents magnitude. CR = Carnegie Ridge; MB = Manabí Basin; BB = Borbón Basin; E = Esmeraldas city and T = Tumaco city. (b and c) Cross sections parallel and perpendicular to the volcanic arc.

where A is the measured maximum amplitude at station j, D is the epicentral distance between i and j, α and β are empirical coefficients and Cj a term which depends of the station j. α, β and Cj are determined for each station by iterative inversion of the n equations (n = 214). Magnitudes of all events are then computed using this empirical law and the recorded amplitudes.

[16] Magnitudes range from 2.2 to 5.5 (see Figure 2 for magnitude distribution). The Gutenberg-Richter magnitude law for the ESMERALDAS data and for a RENSIG data set selected in our study area is shown in the Figure 3b. Both curves, normalized for a period of one year, exhibit a comparable b value of ≈0.8. This illustrates that the seismic rate is identical for both catalogs indicating that our 3 months data is representative of the 15 years RENSIG catalog. We conclude that the NESC subduction zone is currently a steady state system at the observed scales. This implies that the Esmeraldas experiment was carried out during a slowly evolving phase of the seismic cycle, probably corresponding to the interseismic period.

3.4. Focal Mechanisms

[17] We have determined 35 focal mechanisms (Table 3) out of the 263 events located by the ESMERALDAS network. To better constrain these mechanisms we have used a method that combines both P and S wave polarities [*Nakamura*, 2002] (Figures A1 and A2). To read SV and SH polarities, the seismograms were rotated into radial and tangential components. It is more difficult to determine S than P wave polarities because the S wave is perturbed by P wave

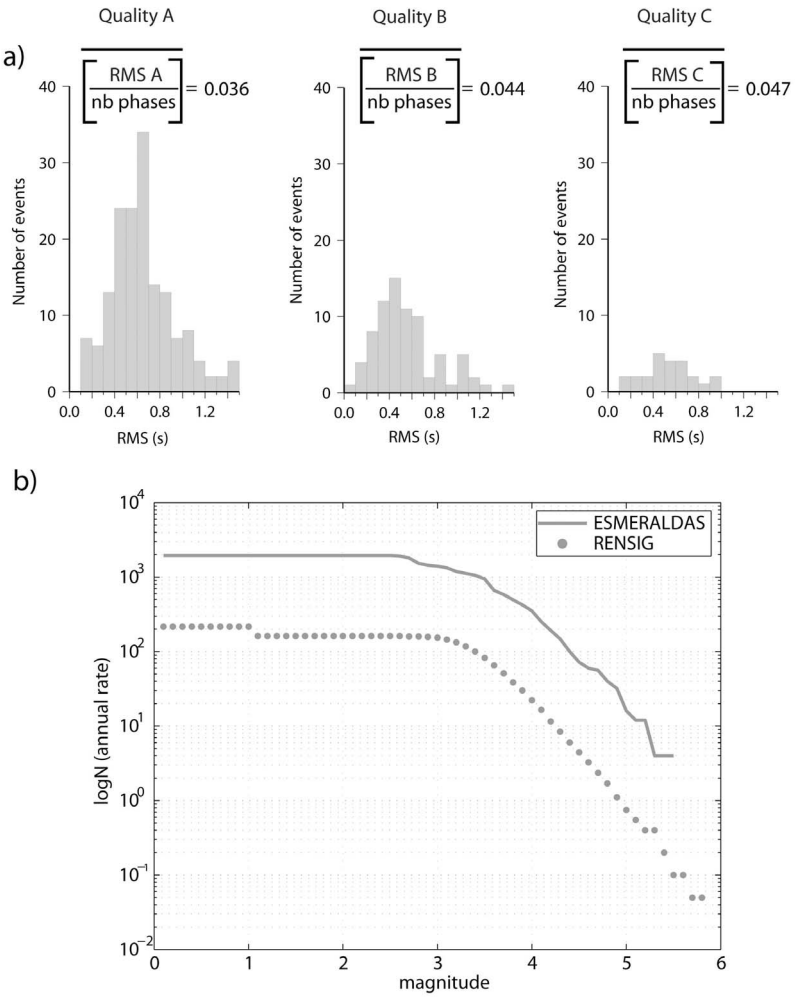

Figure 3. (a) Histograms of residual RMS for class of hypocenters A, B, and C. Average of RMS normalized by the number of phases used to locate the events is calculated for each class of location. (b) Frequency magnitude distributions. Gray solid line represents the Gutenberg-Richter law for the 3 months ESMERALDAS catalog. Gray dashed line corresponds to 20 years permanent Ecuadorian network (RENSIG) records. Data were normalized to one year for comparison.

coda. Low-pass frequency filter have been applied on seismograms to improve S waves polarity measurement. We have used the program FOCMEC [*Snoke et al.*, 1984] that enables to construct focal mechanisms using P and S waves polarities. Details about focal mechanisms determination and all possible solutions compatible with P, SV and SH polarities are presented in Appendix A. The accuracy of the different solutions has been evaluated on each stereographic projection. Some solutions are unequivocally constrained. The worse determinations yield uncertainties of about 20° respectively on azimuth and dip determination, which does not significantly change the nature of the focal solutions.

[18] Available Global Centroid Moment Tensor (GCMT) solutions [*Dziewonski et al.*, 1981] (http://www.globalcmt.org), since the 1979 earthquake and its aftershocks sequence, have been also used to complete our data set (Table 4 and Figures 4, 6, 7 and 9). GCMT related to the Manta crisis are not used because they describe the swarm seismic activity south of the Carnegie Ridge and do not characterize the ongoing deformation along the rupture zones of the megathrust earthquakes.

4. Active Seismic Deformation

[19] In this section we describe the distribution of the seismicity and focal mechanisms within each tectonic unit. According to the location and distances between events and major interfaces resolved by active seismic imaging, the earthquakes are associated to the NAB (15 mechanisms), the subducting oceanic Nazca plate (17 mechanisms) or the ISZ (3 mechanisms). Previous seismic studies determined an angle of about 10° for the top of the oceanic crust immediately west of the trench [*Agudelo*, 2005; *Agudelo et al.*, 2009; *d'Acremont et al.*, 2005; *Gailler et al.*, 2007; *Collot et al.*, 2008]. Taking into account uncertainties on focal depth determination, we consider that the seismicity that is located 5 km above or below the top of the slab defined by these authors belongs to the interplate boundary (ISZ). Events located above the ISZ selection belong to the overriding plate

Table 3. ESMERALDAS Focal Mechanisms

Number	Date	Latitude	Longitude	Depth (km)	Strike (deg)	Dip (deg)	Rake (deg)	HYPOELLIPSE Location Quality	Ml
				North Andean Block					
1	18–03 19h12	0.7094	79.2793	1	128.90	71.25	−68.83	A	4.1
2	04–04 02h25	0.9373	78.4135	8	232.00	41.41	40.89	A	4.0
3	10–04 07h56	0.658	79.2697	18	333.10	82.56	−29.15	A	3.4
4	24–03 04h06	0.4513	78.7345	3	323.60	30.38	−80.08	B	2.5
5	11–05 18h22	0.5196	79.1041	24	170.80	65.60	32.73	A	3.6
6	14–05 21h50	0.2889	79.1049	34	68.70	11.17	63.26	A	3.6
7	14–03 10h15	−0.1251	78.7576	3	342.93	55.15	−3.49	A	3.5
8	02–04 08h58	−0.6553	78.6228	−2	320.40	75.97	−20.91	A	3.4
9	14–04 07h38	−0.0820	78.8655	0	344.40	77.80	21.99	A	3.4
10	27–03 16h31	−0.2791	79.0742	1	183.10	68.37	34.50	A	3.4
11	12–03 10h43	−0.2764	79.1025	4	330.00	60.00	0.00	A	3.6
12	14–05 07h47	0.2264	79.1518	37	302.60	50.14	−56.60	A	4.1
13	11–03 00h19	0.56	79.35	33	52.28	77.76	54.06	B	4.0
14	19–03 07h52	0.6174	79.3291	21	310.90	69.30	−22.21	A	4.0
15	08–06 07h17	0.0757	80.2935	5	291.50	52.84	−16.01	A	3.8
				Slab Bending Related					
16	01–04 16h30	1.5380	80.5523	22	78.19	72.61	−18.25	A	4.2
17	24–05 15h44	2.7817	79.8857	32	340.00	50.00	−90.00	B	2.5
				Subducting Plate					
18	14–04 14h16	0.0853	80.1891	43	178.97	48.73	55.05	A	3.6
19	17–04 13h51	0.1909	80.2988	45	350.00	80.00	−90.00	A	3.7
20	20–04 08h41	0.3659	80.1011	35	298.55	28.9	−29.03	A	3.8
21	17–04 19h57	0.3482	80.1551	37	23.65	80.95	−64.66	A	3.9
22	05–04 10h56	1.4612	78.3845	84	31.16	72.61	42.19	A	3.4
23	07–05 09h38	1.1255	78.9074	58	204.94	20.59	13.47	A	3.3
24	04–06 06h31	0.7930	78.0141	127	246.38	85.67	−59.91	A	4.0
25	07–05 18h38	0.9469	78.9524	75	165.83	85.30	−69.93	A	4.0
26	04–05 16h58	0.7998	79.0423	75	4.68	87.13	34.90	A	3.9
27	04–04 08h53	0.9829	79.3613	71	176.57	78.69	33.34	A	2.9
28	03–06 02h39	0.4855	79.2844	72	58.46	22.27	−62.73	A	3.2
29	18–03 14h22	−0.9481	79.2049	104	231.19	70.71	74.08	A	4.0
30	10–05 07h29	−1.1418	79.3434	74	11.45	27.99	−43.22	B	3.8
31	20–04 07h40	−0.9148	79.6229	79	181.53	31.47	−70.57	B	3.6
32	17–03 14h00	−0.0217	79.9339	65	343.31	71.11	47.21	A	3.8
				Interplate Seismogenic Zone					
33	16–05 09h58	0.2592	80.0999	19	175.02	45.22	82.95	A	4.4
34	16–05 17h14	1.9402	79.2860	13	188.32	51.62	70.72	A	2.5
35	16–05 16h52	1.9038	79.2797	19	195.88	55.61	77.85	A	3.5

and those located beneath, to the downgoing Nazca plate. From 110 km east of the trench events shallower than 50 km depth are considered to be related to the upper plate deformation (Figure 2c). Deeper events are interpreted to belong to the slab.

4.1. Interplate Seismogenic Zone

[20] As explained in the introduction, the NESC margin was the site of 4 great megathrust subduction earthquakes between 1906 and 1979. The rupture areas and zone of maximum slip (asperities) of the three more recent earthquakes (Figure 4a) have been determined by waveform analysis [*Kanamori and McNally*, 1982]. The limits of the rupture areas of the 1942, 1958, 1979 earthquakes are proposed to be governed by structural features of both the downgoing and overriding plates [*Collot et al.*, 2004]. Among these features, the Esmeraldas and Manglares faults affect the NAB and are suggested to delimit the lateral extension of the rupture surfaces (Figure 4a).

[21] Only 16 thrust type focal mechanisms are listed in the GCMT catalog for the NESC subduction zone since 1980 (Table 4 and Figure 4a). Note that focal solutions 33, 34 and 35 computed in this study (Table 3 and Figure 4a) are relatively similar to those of the GCMT catalog. The GCMT solutions do not show a homogeneous distribution along the margin, with 5 of them located north of 2.5°N, i.e., in the northern part of the 1979 earthquake rupture zone, and other 11 located south of 1°N, close or within the 1942 earthquake rupture area (Figure 4a). No GCMT solutions coincide with the area corresponding to the surface rupture of the 1958 earthquake and the southern part of the 1979 surface rupture. ESMERALDAS microearthquake activity is also heterogeneous along the 1942, 1958 and 1979 rupture areas, with 77% of the ISZ activity located south of 1°N, i.e., within the 1942 rupture area, and only 23% in the 1958 and 1979 rupture areas (Figure 4a). Thus, in agreement with GCMT location, we observe a northward gradual decrease of the interplate seismic activity from the 1942 surface rupture to the 1979 rupture area. Note that both ESMERALDAS and GCMT events are scarce or absent over the seismological asperities. The observed interplate seismicity deficit in the northern region cannot be due to the network configuration because the ESMERALDAS OBS network was located nearby. In order to image the "long term" ISZ seismicity pattern we have included data from the ISC catalog, between 1994 (onset of the RENSIG network densification) and 2006. Figure 5

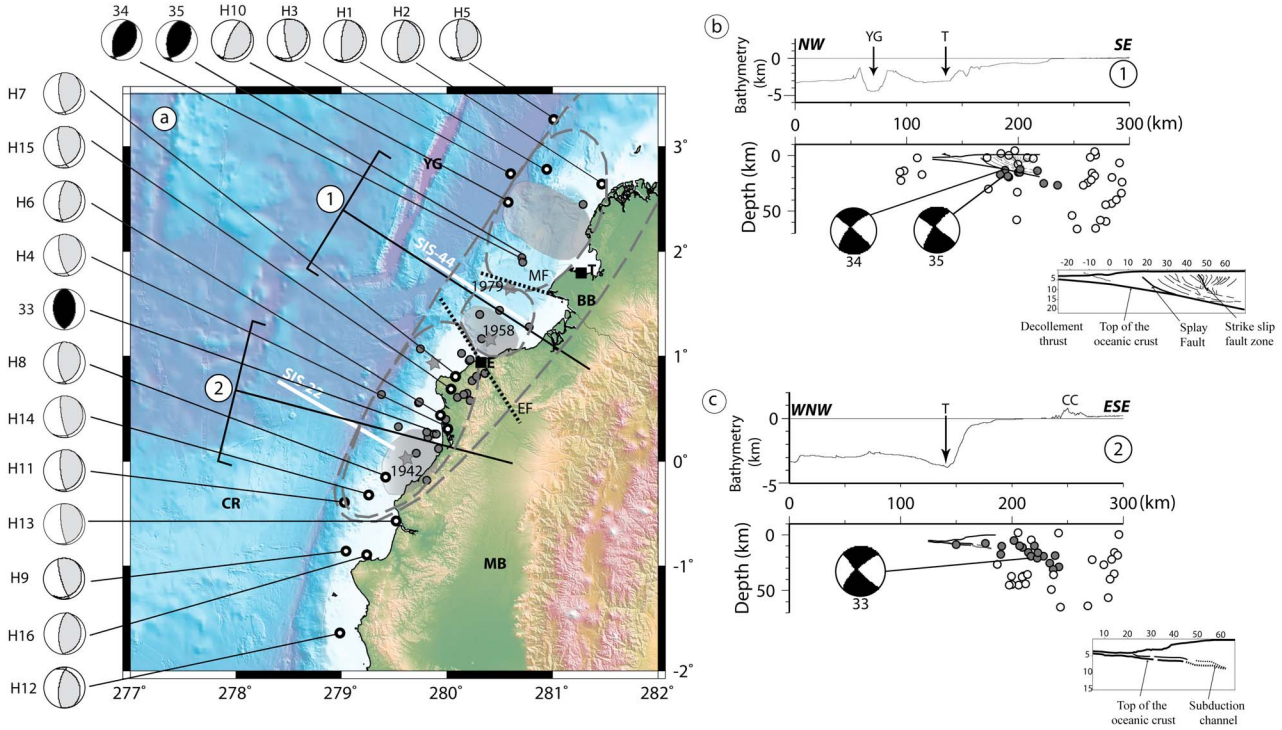

Figure 4. Seismicity related to the Interplate Seismogenic Zone (ISZ) activity. (a) On the map gray dots are for ESMERALDAS data and white dots with bold contour are for the 1980–2009 GCMT catalog solutions. Focal mechanisms are lower hemisphere projection. Compressional quadrants are gray for GCMT solutions and black for ESMERALDAS mechanisms. Identification numbers are reported in Tables 3 and 4. Dashed lines delimit the rupture areas of the four large twentieth century earthquakes, stars are for their epicenters, and gray surfaces represent the seismological asperities of the 1942, 1958, and 1979 earthquakes (see text for references). Black lines on map represent cross section location and width. CR = Carnegie Ridge; BB = Borbón Basin; MB = Manabí Basin; EF = Esmeraldas Fault; MF = Manglares Fault; E = Esmeraldas city and T = Tumaco city. On the (b) northernmost and (c) southernmost cross sections, interpretation of respectively SIS-44 and SIS-22 seismic lines (see the map for profiles location) illustrate the top of the Nazca subducting plate. Interpretation of the SIS-44 wide-angle seismic profile is modified from *Collot et al.* [2008], *Agudelo* [2005], *Agudelo et al.* [2009] and *Gailler et al.* [2007], and sketch of the SIS-22 seismic reflection profile is modified from *d'Acremont et al.* [2005]. Gray dots on the cross sections represent the ESMERALDAS events interpreted as belonging to the ISZ. Open circles represent events interpreted as belonging to the upper plate or to the slab, at a distance from the ISZ.

shows both ESMERALDAS and ISC interplate events distribution in a spatiotemporal diagram, according to surface ruptures and asperities location, in order to visualize the gradual latitudinal decrease of the seismicity as a function of time. Seismicity of ISC catalog essentially occurs along the 1942 rupture area and gradually decreases northward (Figure 5). More specifically, it concentrates preferentially outside asperities. Thus, the 12 year long pattern on ISZ activity confirms the short term ESMERALDAS observations. South of the 1942 asperity, seismicity is organized in three seismic swarms, while northward of it the time distribution is more diffuse, and therefore it can be defined as background seismicity.

[22] Detailed knowledge of the updip limit of the seismogenic zone is a key parameter for seismic and tsunami risk determination. The updip limit corresponds to the transition zone from shallow stable sliding (aseismic) to deeper stick slip (seismogenic) processes along the plate interface [*Tichelaar and Ruff*, 1993]. While the microearthquake activity and extension of large ruptures are not the same physical phenomenon, the microearthquake activity can however help defining the updip limit. Similarly to *Pontoise and Monfret* [2004], our study shows that seismic activity along the plate interface occurs up to a relatively shallow depths of ~10–15 km (Figures 4b and 4c). ISZ focal mechanisms 33, 34 and 35 exhibit thrust fault type solutions (Figures 4b and 4c). Thrust type focal mechanisms depths range from 13 to 19 km, which is consistent with the ~10–15 km depth range for the updip limit that we propose.

[23] The downdip limit of the seismogenic zone is defined as the site of the transition between the interplate brittle domain and a stable sliding behavior [*Tichelaar and Ruff*, 1993]. The eastward extension of the GCMT and ESMERALDAS selected interplate seismicity stops along the eastern border of the 1942 rupture area (Figure 4a). This limit also corresponds to the foothill of the Coastal Cordillera. In our 3 months data set, we observe an interruption of ISZ seismicity at ≈30 km depth, just beneath the Coastal Cordillera (Figures 4b and 4c). *Bollinger et al.* [2004] have interpreted the variation of the interplate seismicity as an effect of the

Table 4. Global CMT Catalog Since 1980

Number	Date	Latitude	Longitude	Depth (km)	Mw	str1 (deg)	dip1 (deg)	rake1 (deg)	str2 (deg)	dip2 (deg)	rake2 (deg)	Mo (dyne/cm)
					Interplate Seismogenic Zone							
H1	07-01-1980 00h33	2,74	−79,06	15	5,3	30	15	114	185	77	84	$9{,}51*10^{23}$
H2	03-09-1980 22h12	2,63	−78,53	37,4	6,1	1	20	85	186	70	92	$1{,}81*10^{25}$
H3	01-08-1982 01h38	2,71	−79,4	15	5,3	41	22	138	171	76	73	$10{,}75*10^{23}$
H4	22-11-1983 14h21	0,31	−79,99	35,2	6,7	33	24	133	167	72	73	$1{,}66*10^{26}$
H5	10-06-1985 03h23	3,24	−78,99	26	5,5	32	19	125	176	74	79	$2{,}52*10^{24}$
H6	19-01-1986 08h03	0,44	−80,06	40	5	31	22	116	184	70	80	$3{,}85*10^{23}$
H7	25-06-1989 20h37	0,81	−79,92	16	6,3	27	25	120	174	69	77	$3{,}39*10^{25}$
H8	02-09-1990 04h26	−0,15	−80,58	21,2	6,2	22	27	115	174	65	78	$2{,}57*10^{25}$
H9	04-08-1991 07h45	−0,86	−80,96	15,6	5,4	33	17	137	164	78	77	$1{,}72*10^{24}$
H10	27-04-1996 23h03	2,47	−79,42	15	6,1	44	15	110	203	76	85	$1{,}56*10^{25}$
H11	16-12-1996 01h46	−0,39	−80,97	27,1	5,5	28	18	123	174	75	80	$2{,}24*10^{24}$
H12	01-07-1998 14h57	−1,65	−81,07	33,7	5,1	33	27	58	188	68	105	$6{,}65*10^{23}$
H13	04-08-1998 18h59	−0,57	−80,48	25,6	7,1	27	15	124	172	78	82	$6{,}37*10^{26}$
H14	28-09-2000 23h23	−0,32	−80,74	15	6,4	34	15	133	170	79	80	$4{,}54*10^{25}$
H15	01-06-2004 15h52	0,69	−79,96	34	5,3	33	28	133	167	70	70	$1{,}33*10^{24}$
H16	24-11-2004 16h19	−0,88	−80,74	33,33	5,1	10	23	95	185	67	88	$5{,}02*10^{23}$
					North Andean Block							
H17	02-01-1981 07h37	0,93	−79,37	15	5,9	26	42	−128	252	58	−61	$9{,}13*10^{24}$
H18	03-06-1987 01h54	0,1	−77,77	15	6,4	198	20	118	348	73	81	$4{,}90*10^{25}$
H19	03-06-1987 04h10	−0,06	−77,84	15	7,1	195	27	98	7	64	86	$6{,}37*10^{26}$
H20	03-06-1987 08h14	0,31	−77,73	15	6	226	40	−166	125	81	−51	$11{,}73*10^{24}$
H21	22-09-1987 13h43	−0,89	−78,24	15	6,3	218	42	147	334	68	53	$4{,}07*10^{25}$
H22	22-09-1987 16h21	−0,98	−78,24	19,4	6	197	42	129	330	59	61	$10{,}66*10^{24}$
H23	11-08-1990 03h00	0,01	−78,15	15	5,3	323	45	53	190	55	122	$9{,}45*10^{23}$
H24	26-12-1992 14h57	−1,15	−77,92	15	5,8	200	46	166	300	80	45	$7{,}00*10^{24}$
H25	28-03-1996 23h03	−1,19	−78,66	15	5,9	8	21	96	182	69	88	$8{,}42*10^{24}$
H26	25-08-1996 14h09	−1,12	−77,99	15	5,4	172	48	130	300	55	54	$1{,}83*10^{24}$
H27	25-03-2000 16h36	1,65	−78,68	33,6	5,2	327	27	27	213	78	115	$7{,}58*10^{23}$
H28	08-10-2000 20h12	0	−78,07	15	5,1	342	42	90	162	48	90	$5{,}49*10^{23}$
H29	13-09-2003 18h33	−1,01	−78,51	31,5	5,3	233	70	−163	137	74	−21	$1{,}01*10^{24}$
H30	28-03-2004 08h41	−1,12	−78,47	12	5,2	193	50	135	316	57	50	$0{,}89*10^{24}$
H31	15-04-2004 19h06	−0,91	−78,42	18,3	4,9	198	41	128	332	59	62	$3{,}08*10^{23}$
					Subducting Plate							
H32	08-10-1980 22h01	−1,23	−77,53	192,1	6	115	16	−117	323	76	−82	$12{,}40*10^{24}$
H33	04-10-1981 20h03	−1,44	−77,38	208.5	5.4	170	19	−38	296	78	−105	$1{,}65*10^{24}$
H34	03-11-1981 07h02	−1,78	−78,37	145,3	5,9	133	28	−99	323	62	−85	$8{,}17*10^{24}$
H35	20-05-1982 12h10	−1,41	−78,25	181,1	5,3	176	19	−36	300	79	−105	$10{,}04*10^{23}$
H36	28-01-1986 06h51	−1,84	−77,76	166,3	5,4	157	25	−51	295	71	−107	$14{,}03*10^{23}$
H37	18-12-1987 05h01	−1,26	−77,91	172,9	5,5	142	25	−76	306	66	−97	$2{,}18*10^{24}$
H38	15-09-1988 18h48	−1,25	−78,01	169	6,2	121	28	−109	322	64	−80	$2{,}32*10^{25}$
H39	25-01-1994 05h41	−1,72	−77,79	154,3	5,4	195	35	−36	316	70	−120	$1{,}62*10^{24}$
H40	28-01-1996 00h28	−1,79	−77,71	149	5,3	149	24	−63	300	68	−102	$11{,}13*10^{23}$
H41	26-04-1999 18h17	−1,5	−77,83	164,2	6	169	33	−49	304	66	−113	$13{,}47*10^{24}$
H42	28-08-1999 12h40	−1,36	−77,75	198,2	6,2	122	18	−107	320	73	−85	$2{,}51*10^{25}$
H43	21-06-2005 10h03	−1,86	−78,02	166,1	5	131	16	−94	316	74	−89	$3{,}43*10^{23}$
H44	09-11-2005 11h33	−1,2	−77,1	247,4	5,9	179	14	−39	308	81	−101	$7{,}91*10^{24}$
H45	23-12-2005 21h47	−1,59	−77,76	196,8	6,1	120	21	−107	318	69	−84	$1{,}87*10^{25}$
H46	31-10-2006 09h55	−1,53	−78,04	177,5	5,4	137	29	−80	306	61	−95	$1{,}63*10^{24}$
H47	06-01-2007 06h27	−1,52	−78,09	164,4	5	127	40	−102	322	51	−80	$3{,}55*10^{23}$
H48	13-02-2007 14h56	−1,6	−78,05	175,8	5,6	139	25	−95	325	65	−88	$2{,}82*10^{24}$
H49	23-02-2007 14h12	−1,58	−78,08	160,1	5	95	52	−154	348	70	−41	$4{,}43*10^{23}$
H50	28-03-2007 20h57	−1,6	−77,81	191,5	5,3	104	24	−124	321	70	−76	$0{,}95*10^{24}$
H51	21-07-2007 18h58	−1,66	−78,3	158,7	5,2	132	23	−101	325	68	−85	$0{,}88*10^{24}$
H52	04-07-2008 06h02	−1,58	−77,91	193,4	5,2	122	32	−119	335	62	−73	$0{,}85*10^{24}$
H53	01-05-2009 00h34	−1,74	−77,66	194,9	5,1	153	21	−62	304	71	−100	$5{,}86*10^{23}$
					Slab Bending Related							
H54	11-05-1980 09h26	1,95	−80,32	15	5,5	330	56	172	65	83	34	$2{,}00*10^{24}$
H55	03-01-1981 01h23	2,13	−78,95	15	5,9	26	42	−128	252	58	−61	$9{,}13*10^{24}$
H56	07-01-1981 07h01	1?72	−79,31	15	5,5	32	33	−114	240	60	−75	$2{,}64*10^{24}$
H57	07-07-1981 10h25	2,77	−79,87	15	5,3	16	43	−78	180	48	−101	$1{,}08*10^{24}$
H58	12-02-1989 20h03	2,41	−79,44	33	5,1	340	46	−116	195	50	−66	$5{,}64*10^{23}$
H59	09-09-1989 01h40	1,92	−79,53	15	5,7	1	29	−123	218	66	−73	$4{,}16*10^{24}$
H60	26-11-1994 04h48	2,65	−79,32	15	5,2	357	37	−114	206	57	−73	$9{,}43*10^{23}$
H61	10-10-1995 17h29	1,64	−78,97	55,1	5,1	253	46	104	53	46	76	$5{,}68*10^{23}$
H62	05-10-1997 00h55	2,15	−79,56	15	5,3	345	25	−140	218	74	−71	$10{,}53*10^{23}$
H63	11-03-1999 16h56	2,97	−79,86	33	4,9	27	43	−61	170	53	−115	$2{,}78*10^{23}$
H64	03-08-2005 21h20	2,64	−79,46	13,17	4,9	34	35	−64	183	59	−107	$2{,}59*10^{23}$

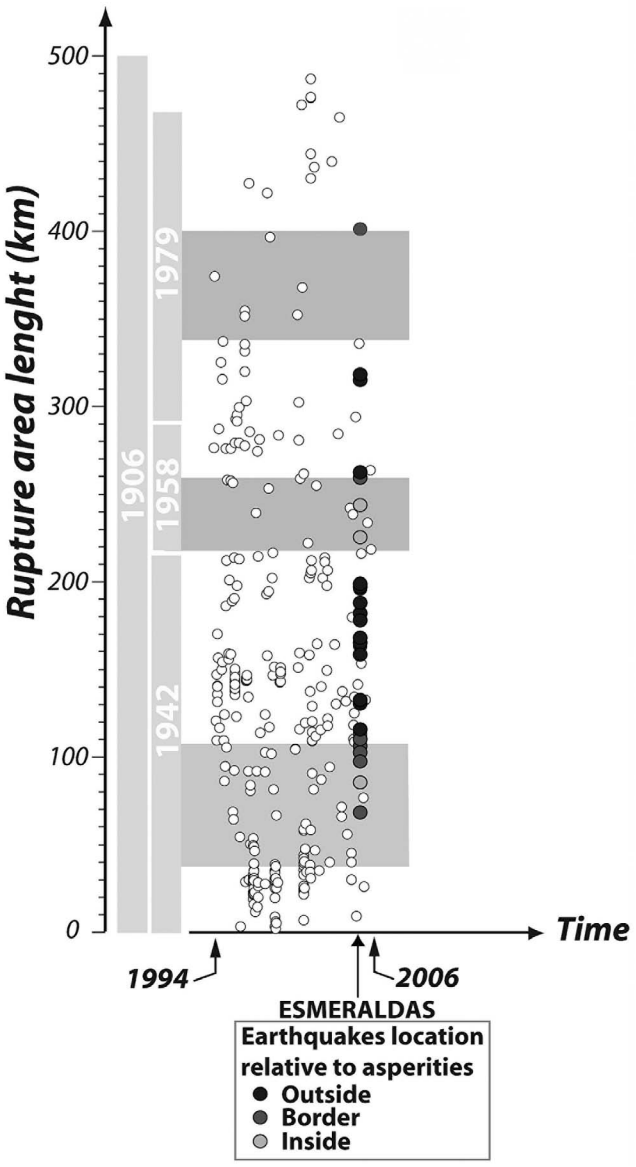

Figure 5. Space-time diagram showing both the ISC (white circles) and ESMERALDAS (gray to black circles) events distribution. Light gray areas represent large earthquakes rupture areas location, and dark gray areas represent asperities position.

influence of an overlying relief on the deviatoric stresses. They showed that the interplate seismicity along the Main Himalayan Thrust ends beneath the high topographic range. Due to the spatial coincidence in our study area, between the three months "seismic gap" and the Costal Cordillera location, we suggest that the Coastal Cordillera could play a role on the interplate coupling and might control the location of the downdip limit of the ISZ, which in our case would be located at ≈30 km depth (Figures 4b and 4c). This is consistent with the hypocentral location of the 1979 event, defined at 24.3 and 37.5 km depth, respectively by *Engdahl and Villaseñor* [2002] and *Mendoza and Dewey* [1984]. The 30 km depth value is also a little shallower than the global average (40 ± 5 km depth) proposed by *Tichelaar and Ruff* [1993], based on rupture determination of large earthquakes.

4.2. Subducting Plate

4.2.1. Outer-Rise Seismicity

[24] Bathymetric and seismic reflection analysis along the NESC margin evidence the presence of normal faults on the incoming plate [*Ratzov et al.*, 2010] related to the oceanic plate bending as it enters the subduction zone [*Chapple and Forsyth*, 1979]. Seaward seismic activity immediately west of the trench (Figures 6a and 6b) likely reflects this bending-related normal fault activity. Focal mechanisms 16 and 17 (Table 3 and Figures 6a and 6b) support this model, as these two solutions are located west of the trench, respectively at 22 and 32 km depth and show T axes in agreement with ENE-WSW and NW-SE extension. According to their location and to their mechanism type, GCMT solutions H54 to H64 (Table 4 and Figure 6a) are also interpreted to be reliable outer-rise seismicity. The orientation of the T axis is not truly normal to the trench and we suggest that the deformation could happened along preexistent structures of the oceanic plate, as it is the case for the mechanisms 16, 17, H54, H57 and H63 that occurred close to the Yaquina graben (Figure 6a). We note that there is no outer rise seismicity in the Carnegie Ridge. This is probably due to a different rheological behavior of the thicker subducting crust.

4.2.2. Wadati-Benioff Plane Geometry

[25] The Wadati-Benioff plane allows characterizing the deep slab geometry and reveals the downgoing plate deformation. Associated slab deformation events are presented both in map and cross sections in Figure 6. Distribution of the intermediate depth seismicity defines two different domains, north and south of 0.5°N. As the seismological network covers both domains, the hypocentral distribution is not biased by the network configuration, which allows to determine the dip angle of the downgoing plate and to define the Wadati-Benioff plane geometry.

[26] The cross section A crosscuts the northern domain (Figure 6b), whereas profile B intersects the southern area. North of 0.5°N, the seismicity is mainly located beneath the fore-arc region, and stops beneath the western foothill of the Cordillera, at a distance of ≈170 km eastward from the trench (Figure 6a). The slab geometry is well defined down to ≈100 km depth (Figures 6a and 6b). To the south, deep intraslab seismicity extends down to ≈140 km depth beneath the cordillera, at ≈300 km eastward from the trench (Figures 6a and 6c).

[27] No difference in terms of slab dip is observed between the two cross sections. Both in the northern and southern domains the slab is dipping eastward with an angle of ~25° (Figures 6b and 6c). This slab dip is lower than the 35° proposed by several authors [*Pennington*, 1981; *Guillier et al.*, 2001; *Pontoise and Monfret*, 2004]. Moreover the ESMERALDAS locations do not show any evidence for the presence of a 100 km deep flat slab facing the Carnegie Ridge under the northern Ecuadorian margin, as postulated by *Gutscher et al.* [1999]. Nevertheless, these authors noticed the lack of seismological constraints, using only the Engdahl and Harvard catalogs, to support this hypothesis. Conversely, our study evidences the presence of a continuous seismicity along the slab, south of 1°N (Figure 2). Besides, using the

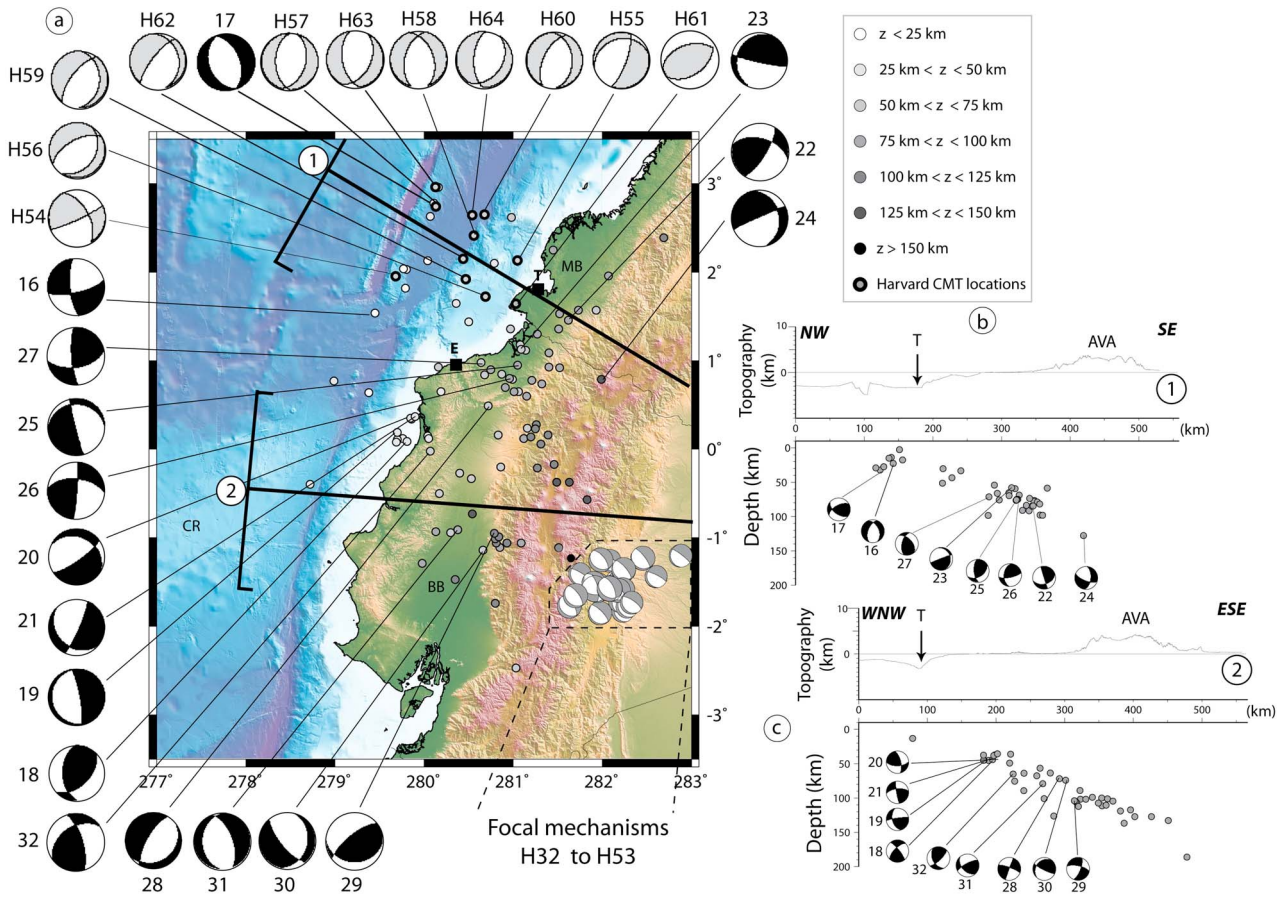

Figure 6. Downgoing Nazca plate deformation. (a) GCMT (bold contour circle) and ESMERALDAS locations (color of circles indicates focal depth) that belong to the slab. Focal mechanisms are lower hemisphere projection. Black (ESMERALDAS solutions) and gray (GCMT solutions) quadrants are the compressional ones. See Tables 3 and 4 for details about mechanisms solutions. Black lines represent cross section location and width. CR = Carnegie Ridge; MB = Manabí Basin; BB = Borbón Basin; E = Esmeraldas city and T = Tumaco city. (b and c) Northern and southern cross sections presenting locations and focal mechanisms of the ESMERALDAS data set. Focal mechanisms are projected in cross section.

NEIC database, we can make the assumption that the 150–200 km deep seismic cluster located inland at about 350 km from the trench is in the continuity of our data (Figure 1b). This would imply a continuous depth extension of the Wadati-Benioff plane down to about 200 km at least. Taking into account that flat slab are world wide observed at depths shallower than 150 km [*Gutscher et al.*, 2000], the slab geometry defined by the distribution of seismicity beneath Ecuador is not consistent with the flat slab hypothesis.

4.2.3. Subducting Plate Deformation

[28] At depths ranging between 80 and 150 km, we have calculated 15 focal mechanisms (18 to 32; see Table 4) corresponding to intraslab seismicity (Figures 6b and 6c). These intraslab mechanisms are heterogeneous and generally present both subvertical and subhorizontal fault planes solutions. A commonly invoked possible mechanism to explain the intermediate depth seismicity is dehydration imbrittlement [*Hacker et al.*, 2003]. *Ranero et al.* [2005] studied several subduction zones and their results support that intraslab intermediate depth earthquakes may occur along subvertical reactivated faults created originally by the bending of the oceanic plate near the trench. *Warren et al.* [2008] identified subhorizontal fault planes solutions deeper than 100 km depth, in the Middle America Trench. They propose that, at these depths, the local stress field, influenced by the slab pull force, can change in the slab, allowing the formation of the new subhorizontal fault planes. ESMERALDAS data analysis we have performed do not allow us to discriminate the focal plane, and consequently to support one of the two intraslab intermediate depth deformation pattern described above.

4.3. North Andean Block Deformation

[29] Due to the poor azimuthal coverage, upper plate crustal seismicity in the fore-arc region is not well sampled. The few crustal events have no reliable depth [*Guillier et al.*, 2001; *Pontoise and Monfret*, 2004] and these authors suggest that the reason is that the NAB acts as an undeforming body, moving to the northeast along the Dolores Guayaquil Megashear. Our results show that the fore-arc region is seismically active and associated with significant along strike variations (Figure 7). The upper plate seismicity stretches from the surface down to at least 40 km depth (Figure 2), at least in the eastern part of the NAB. This depth limit is

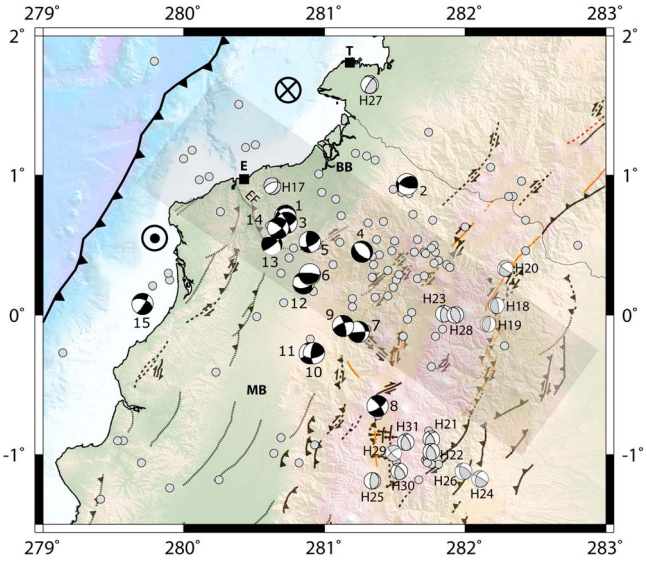

Figure 7. Upper plate deformation and events locations from ESMERALDAS experiment (gray circles) and GCMT catalog data. Focal mechanisms are lower hemisphere projection (black compressional quadrants = ESMERALDAS solutions; gray compressional quadrants = GCMT solutions). Neotectonic structures are from *Eguez et al.* [2003]. Gray stripe underlines denser seismic activity, coinciding with the limit between a northern subsident segment and a southern uplifted segment. MB = Manabí Basin; BB = Borbón Basin; E = Esmeraldas city and T = Tumaco city.

interpreted to represent the maximum depth extent of the brittle domain. As the margin is composed of several accreted blocks [*Kerr et al.*, 2002; *Cediel et al.*, 2003], we suggest that the underthrusting and associated block pile up processes might have contributed to thicken the overlying plate brittle domain. This deep brittle behavior is observed in regions with thick-skin tectonic style, as observed for example, in the Andean foreland in Argentina [*Jordan et al.*, 1983; *Regnier et al.*, 1992; *Pardo et al.*, 2002]. Thick brittle domains in the upper plate are frequent in tectonic context involving collision, strong coupling along the plate interface and/or subduction segment with flat slab. This usually implies a compressional stress regime in the crust of the upper plate, as it is the case for the coastal block of North Ecuador, up to the foothill cordillera [*Daly*, 1989; *Benítez*, 1995; *Jaillard et al.*, 1995; *Jaillard et al.*, 1997]. The comparison with the neotectonic map of Ecuador [*Eguez et al.*, 2003] also indicates that this deformation is probably accommodated along ~N30 strike slip fault systems and reverse faults (Figure 7). This is in agreement with the calculated strike slip motion of focal mechanisms 5, 7, 8 and 9 (Table 3 and Figure 7) located close to previously identified strike slip faults.

[30] Our 3 months data set shows common features with the NEIC catalog concerning the seismicity in the fore-arc basins, with only very few recorded earthquakes in both the Manabí and Borbón Basins (Figures 1b and 7). The seismic activity of the NAB appears to be more concentrated in a roughly 100 km wide stripe stretching over the Esmeraldas region and oriented NW-SE (Figure 7). This seismic zone coincides with a variation in the orientation of the Andes trend that changes from a N-S direction south of ~0.3°N to a NE-SW direction north of this limit. This intensive deformation stripe is also located along the narrow topographic high that separates the Borbón and Manabí Basins (Figures 1 and 7). It is also the site of a sharp change in the tectonic deformation style of the margin, varying from the Esmeraldas uplifted segment, from Esmeraldas to the North Peru, to the subsident Manglares segment, from Esmeraldas to Buenaventura (Colombia) [*Deniaud*, 2000; *Pedoja et al.*, 2006b].

5. Discussion

5.1. Interpretation of Interplate Seismicity Distribution

[31] The dense ESMERALDAS onshore-offshore network, combined to permanent stations, allowed to record moderate seismic activity that had never been previously recorded along the NESC coastal region. The notable increase of the magnitude threshold observed ($2.2 < M_l < 5.5$) by the network is a key to improve our knowledge on active deformation processes as compared with the information provided by global databases (NEIC, GCMT and ISC). The latter only show the strongest activity of the NESC segment of the north Andean subduction zone (Figures 1b, 2a and 9). *Trenkamp et al.* [2002] and *White et al.* [2003] interpreted GPS measurements in the study area as an evidence for a high coupling along the ISZ. Strongly coupled areas are likely the sites of eventual asperities, defined as main shock maximum slip area [*Lay and Kanamori*, 1981; *Lay et al.*, 1982; *Kanamori*, 1986]. In the model of *Scholz* [1988, 1990], the interplate seismicity distribution is characterized by a sequence of different patterns that followed each other in time and space: the main shock is followed by an aftershock sequence (A) that is later followed by a period of quiescence (Q_1) that lasts for 50–70% of the recurrence period of the main shock. Then there is a general increase in background seismicity over the whole region (B). The subsequent principal rupture is preceded by a succession of short periods of quiescence (Q_2 and Q_3) and foreshock activity (F) immediately around the area of maximum slip. In the following we discuss the spatiotemporal organization of the interplate seismicity during the twentieth century main shocks sequence in the light of this model [1988, 1990] (Figures 5 and 8). We interpret the current interseismic ISZ activity (ESMERALDAS and 1994–2006 ISC records) as representing the background seismicity (B) (Figure 8). *Bollinger et al.* [2004] proposed a model in which the microseismicity along a plate interface is driven by stress buildup during the interseismic period. Following this hypothesis, the northward gradual decrease of the interplate seismic activity along the 1942 to 1979 rupture areas could be related to a northward decrease of accumulated interplate stress along the plate interface. This model therefore suggests that interplate microseismic activity and eventually stress buildup depends on the chronology of the twentieth century large earthquakes, with a higher rate of seismicity and stress loading along the rupture area of the oldest earthquake (1942).

5.2. Effect of Carnegie Ridge Subduction

[32] Subduction of aseismic ridges with thickened oceanic crust is one of the models commonly proposed to explain slab flattening. *Gutscher et al.* [2000] showed the correlation between subduction of ridge and flat slab along the Andean

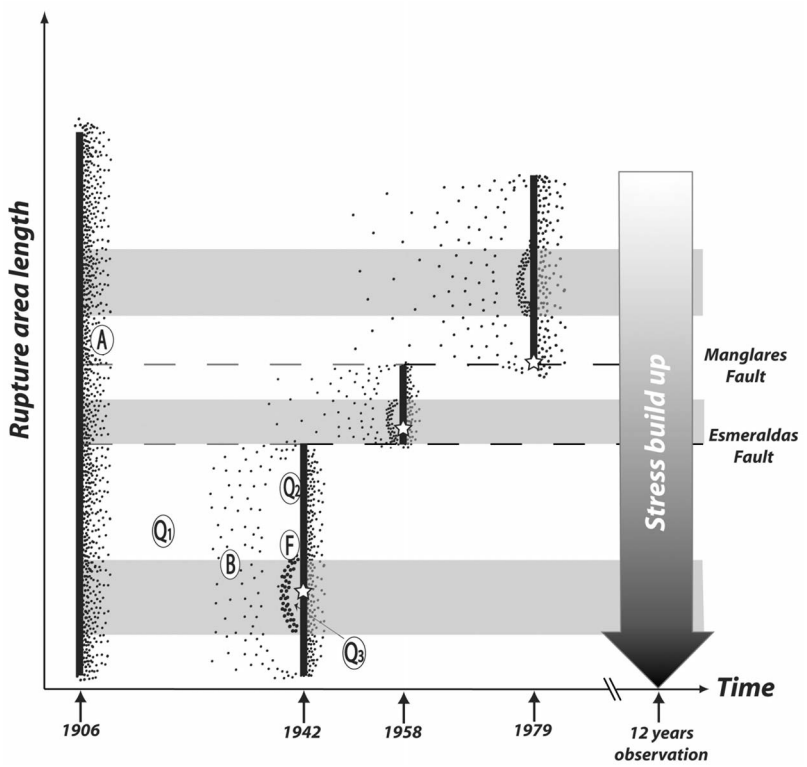

Figure 8. Schematic space-time diagram illustrating various patterns of interplate seismicity that may be recognized during the seismic cycle, adapted to the 4 main shocks sequence along the NESC margin (modified from *Scholz* [1988]). Large black lines correspond to the rupture areas, stars are for megathrust earthquakes epicenters, and gray areas represent asperities location through time. Dashed lines show structural heterogeneities that may limit the rupture zones of the great earthquakes (the Manglares and the Esmeraldas faults [after *Collot et al.*, 2004]). A = aftershocks sequence, Q_1 = first quiescence period, B = background seismicity, Q_2 = second period of quiescence, F and Q_3 precede a megathrust earthquake and correspond respectively to the foreshocks and to the third period of quiescence. Large arrow represents the northward gradual decrease of the interplate background seismicity evidenced by ISC (1994–2006) and ESMERALDAS data.

margin, including the well-known Chile and Peru flat slabs and the proposed Ecuadorian one. Our results show that facing the Carnegie Ridge, the Wadati-Benioff plane dips with a constant dip angle of 25° from 30 km down to 140 km depth. The proposed ages for the onset Carnegie Ridge subduction vary generally from 1 to 3 My [*Lonsdale*, 1978; *Sallarès and Charvis*, 2003; *Cantalamessa and Di Celma*, 2004; *Michaud et al.*, 2009], but some authors have proposed older ages reaching ≈8 My [*Daly*, 1989; *Gutscher et al.*, 1999]. Figure 9 presents the inferred continuation for the Carnegie Ridge prolongation from 8 My [*Gutscher et al.*, 1999] and 1.5 My [*Michaud et al.*, 2009]. Recent analog models suggest that slab flattening process requires an average of 10 My of ridge subduction to occur [*Espurt et al.*, 2008]. Our results do not show evidence of flat slab and therefore confirm that the onset of Carnegie Ridge subduction is younger than 10 My. From geological analysis, *Ramos and Folguera* [2009] propose that the Ecuadorian margin may constitute an incipient flat slab subduction segment. Along the actual well known Andean flat slab segments (Bucaramanga, Peruvian and Pampean segments), the authors characterize geological processes linked to shallowing and steepening of the subduction zones and their geological consequences. Normal to flat slab transition seem to be associated with a series of events such as the migration of the volcanic front and lateral expansion of the arc magmatism, the uplift of the Main Andes and compressive tectonic and uplift in the foreland area, as it observed in Ecuador [*Winkler et al.*, 2005; *Christophoul et al.*, 2002; *Bès de Berc et al.*, 2005]. To agree with both geological and seismological observations we suggest that the slab dip angle may be currently in the process of shallowing. It is clear that instrumental seismicity cannot constrain this proposed long-term flattening process. Instead, it clearly shows that currently the slab is not flat between 0 and 140 km facing the Carnegie Ridge.

[33] Flat slab zones along the Andean margin coincide with a volcanic gap [*Jordan et al.*, 1983]. This fact has been explained by several authors based on thermomechanical models as a consequence of the alteration of the thermal structure of the margin, by bringing cold oceanic lithosphere to a position beneath the upper lithosphere, where typically hot asthenosphere is present [*Gutscher et al.*, 2000; *Wagner et al.*, 2005; *Gerbault et al.*, 2009]. The volcanic arc of the margin is one of the most active chains of the world, with numerous active volcanoes. Evidences for geochemical changes from calc-alkaline to adakitic magmas have been

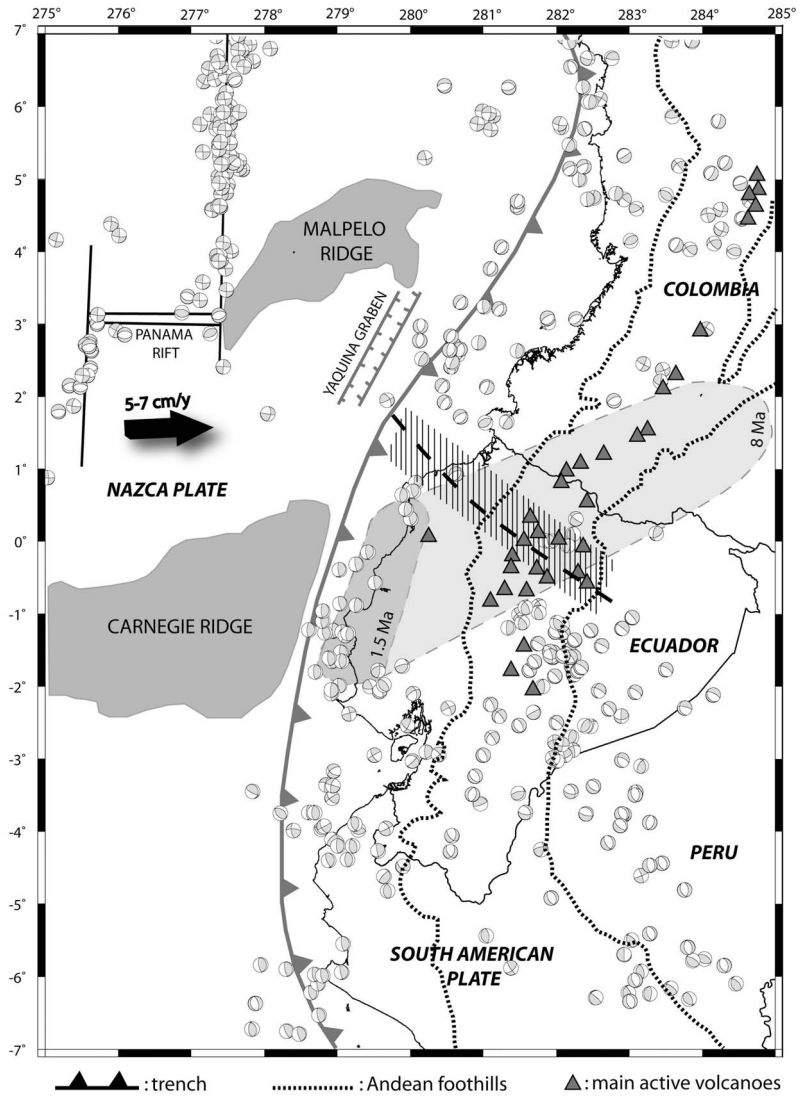

Figure 9. Geodynamical sketch of the North Andean margin. Light and dark gray areas represent respectively the 8 Ma Carnegie Ridge prolongation proposed by *Gutscher et al.* [1999] and the 1.5 Ma Carnegie Ridge prolongation as suggested by *Michaud et al.* [2009]. Focal mechanisms are the GCMT solutions in lower hemisphere projection (from 1980 to 2009). Shaded rectangle stripe underlines the major deformation zone in the NESC upper plate (from this study), and dashed line shows the Pastaza-Esmeraldas boundary [*Hall and Wood*, 1985].

observed in different volcanic complexes along the Ecuadorian arc. The proposed ages of this major geochemical change range from 1.6 My to 0.1 My [*Samaniego et al.*, 2002; *Bourdon et al.*, 2003; *Samaniego et al.*, 2005]. The adakitic geochemical signature of the magma requires either unusually high temperatures allowing fusion of oceanic crust at shallow depths (<120 km) or a severe contamination by underplated basaltic crustal melts [*Monzier et al.*, 1997]. To explain the presence both of volcanism and flat slab, *Gutscher et al.* [1999] proposed that the adakitic signature of the magmas in Ecuador is the result of partial melting at depth of the young thickened Nazca plate. They linked the occurrence of adakitic magmatism with the possible presence of two lithospheric tears that would separate the eventual flat slab induced by the Carnegie Ridge and two slab segments of steep dip, north and south of the ridge. At the edges of the tears, the contact between the oceanic crust and the hot asthenosphere would have produced melting of the oceanic lithosphere and thus could explain the adakitic magmas observed in Ecuador. Our results do not support a flat slab (Figure 6) and led to reconsider the presence of the lithospheric tears and consequently the mode of adakitic magma generation. Based on the seismological observations presented in this study, we suggest that the crust of the overriding continental plate is rather thick, as evidenced by the deep seismicity (down to 40 km depth; Figure 2). This led us to suggest that the adakitic signature of the magma could be more likely related with partial melting of underplated oceanic material at the base of the overriding plate, as proposed by *Garrison and Davidson* [2003] and *Bryant et al.* [2006].

[34] One of the effects of the Carnegie Ridge subduction is to tectonically segment the margin, by producing uplift facing

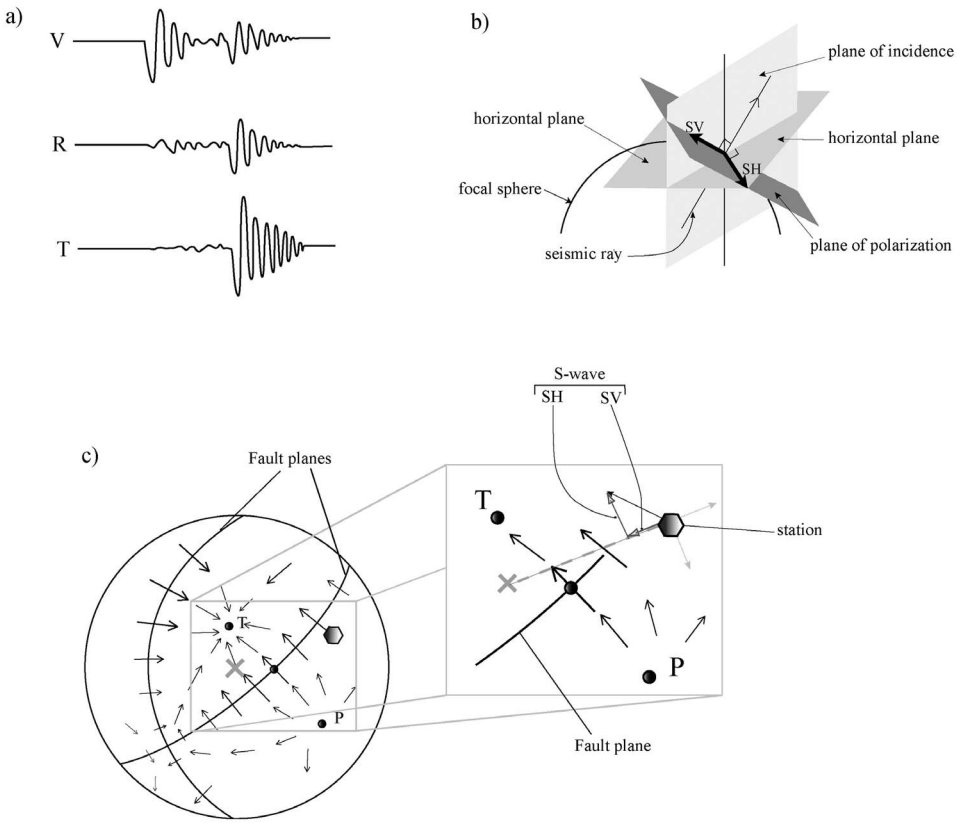

Figure A1. Use of S wave polarity to constrain focal mechanisms. (a) Scheme of 3 components seismogram. The horizontal components have been rotated. (b) Polarization of the SV and SH waves on the focal sphere. (c) Diagram for the radiation pattern of the transverse component of displacement due to a double couple (modified from *Aki and Richards* [1980]). This diagram is a view of the radiation pattern over a whole sphere centered on the origin, and arrows (with varying size and direction) in the spherical surface denote the variation of the transverse motion. The stereographic (equal-angle) projection has been used.

the ridge and subsidence north of it [*Deniaud*, 2000; *Pedoja et al.*, 2006b]. This limit between these two segments coincides with the upper plate active deformation along a NW-SE 100 km wide stripe evidenced in this study. This seismic stripe runs from the Esmeraldas city region up to the Western Cordillera (Figures 7 and 9), connecting the sites where both the Andes and the trench changes their trend. Using LANDSAT images and geological studies, *Hall and Wood* [1985] proposed a NW-SE trending major transverse structure, cutting through the Andes and into the Amazon Basin, in the same area of the observed seismicity stripe, and called it the Pastaza-Esmeraldas boundary (Figure 9). They also noted the occurrence of shallow seismic activity with apparent left-lateral motion along the boundary [*Stauder*, 1975; *Hall and Yepes*, 1982]. This is in agreement with focal mechanisms 3, 7, 9 and 14 computed in this study if we consider that the nodal plane trending NW-SE is the fault plane (Figure 7).

6. Conclusion

[35] The good coverage of the ESMERALDAS onshore-offshore seismological network has allowed us to precisely determine the seismicity distribution and to characterize the associated deformation from the trench to the Cordillera along the NESC margin. Our results suggest the following:

[36] 1. The distribution of the seismic activity along the Interplate Seismogenic Zone is consistent with that expected during the interseismic period of the seismic cycle. Spatial distribution is not homogeneous along strike. We propose that the gradual decrease of interplate seismicity from the oldest to the youngest megathrust earthquake rupture area could be caused by a difference of stress buildup along strike.

[37] 2. The hypocentral distribution shows that slab dip along the NESC is ≈25°. The Wadati-Benioff plane is well defined down to 100 km and 140 km depth, respectively for the northern and southern segments of the region under study. We found no evidence of flat slab facing the Carnegie Ridge, where the Wadati-Benioff plane is continuous from the trench to 300 km landward.

[38] 3. The fore-arc region is undergoing present-day thick brittle deformation down to 40 km depth, indicating the presence of a rather thick brittle crust. This deformation zone extends along a roughly 100 km wide stripe, oriented NW-SE, coincident with the change of trend of the Andes.

Appendix A

[39] Figure A1 shows the use of S wave polarities for focal mechanisms determination. Figure A2 shows focal mechanisms solutions.

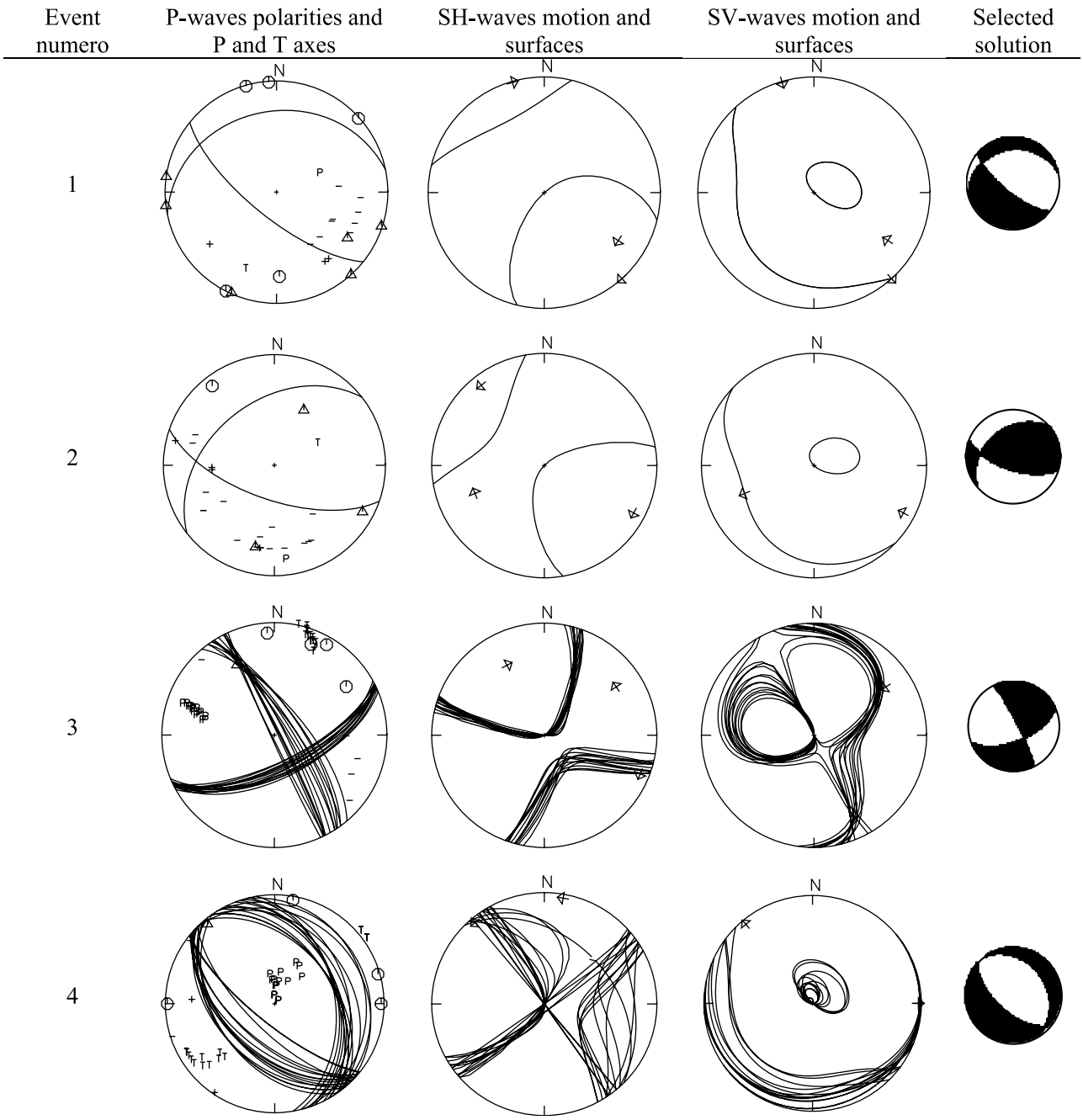

Figure A2. Focal mechanisms construction. Concerning the P wave polarities, representations are in lower hemisphere projection. Triangles are for impulsive dilatation and minus signs are for emergent dilatation; circles are for impulsive compression and plus signs are for emergent compression. Concerning the use of SV and SH polarities, arrows indicate S wave motion, deduced from the read polarity, on the focal sphere.

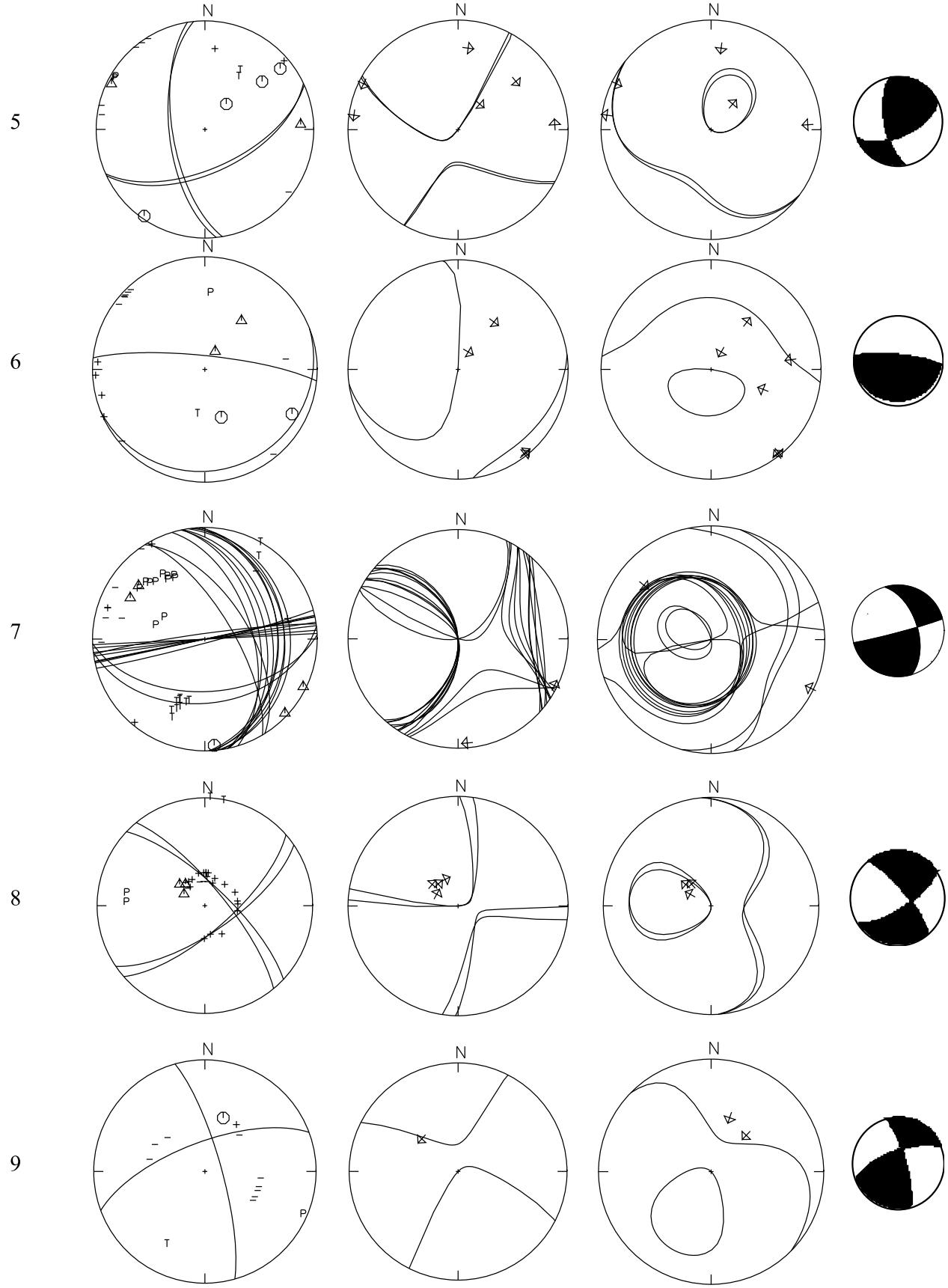

Figure A2. (continued)

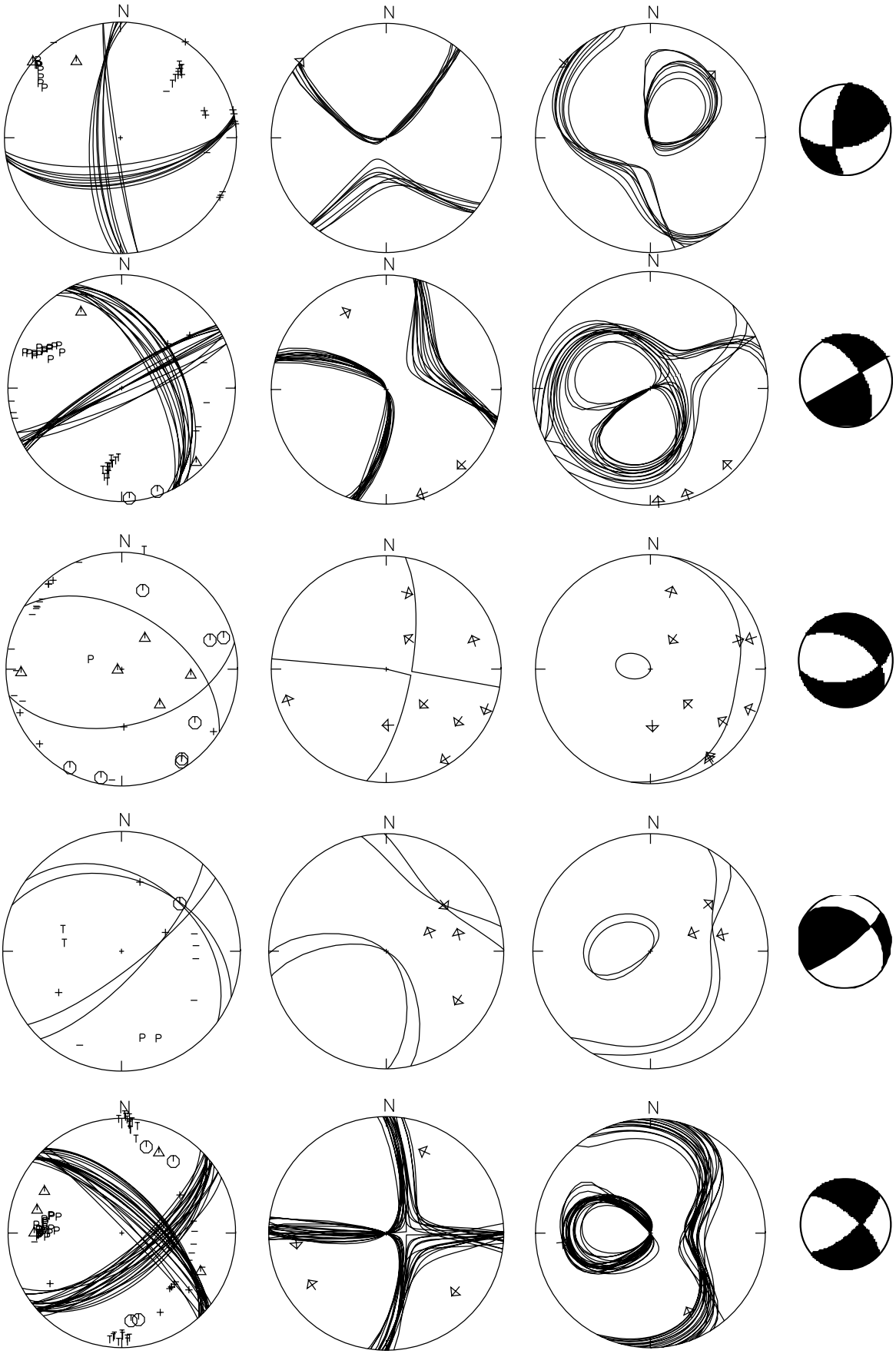

Figure A2. (continued)

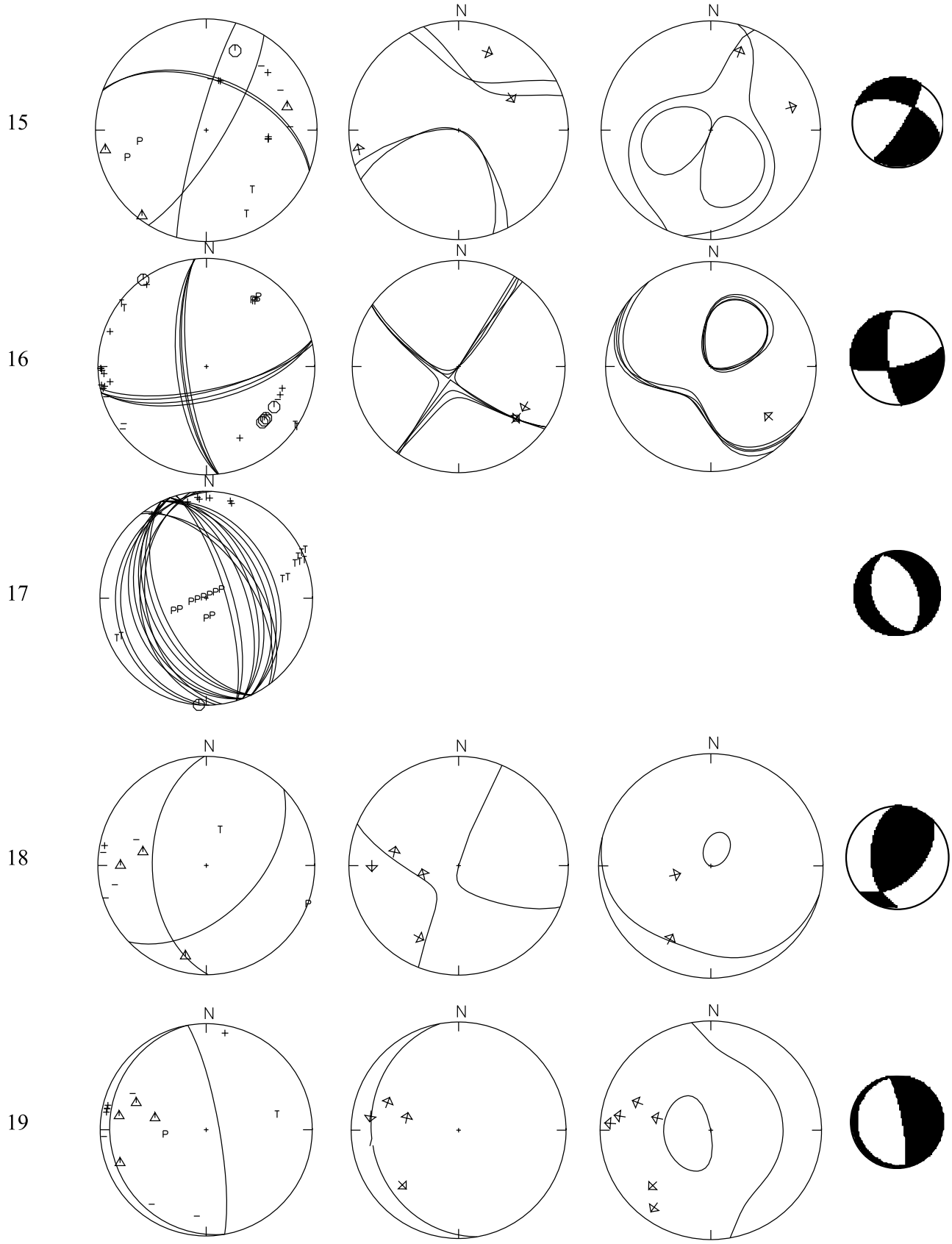

Figure A2. (continued)

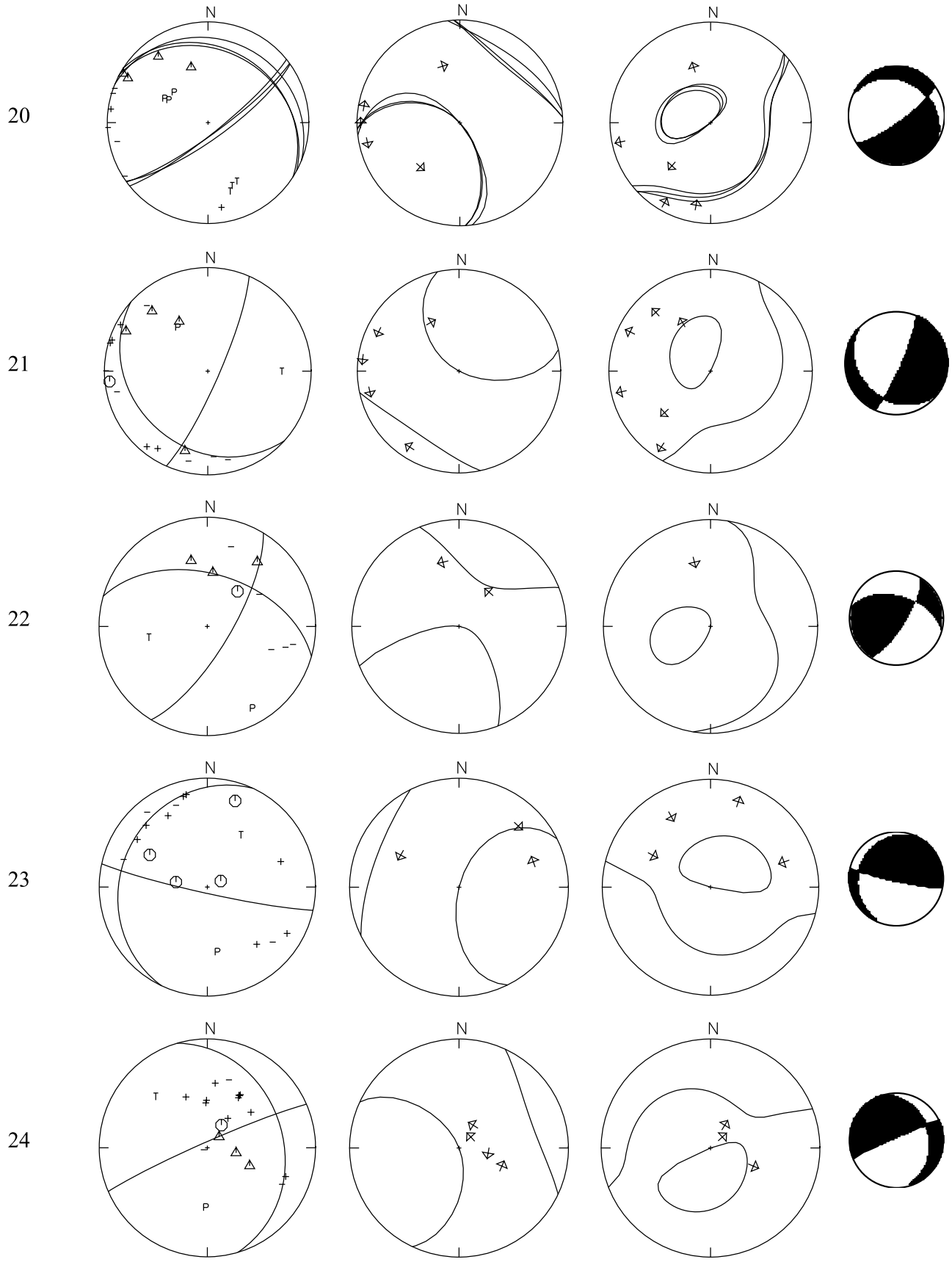

Figure A2. (continued)

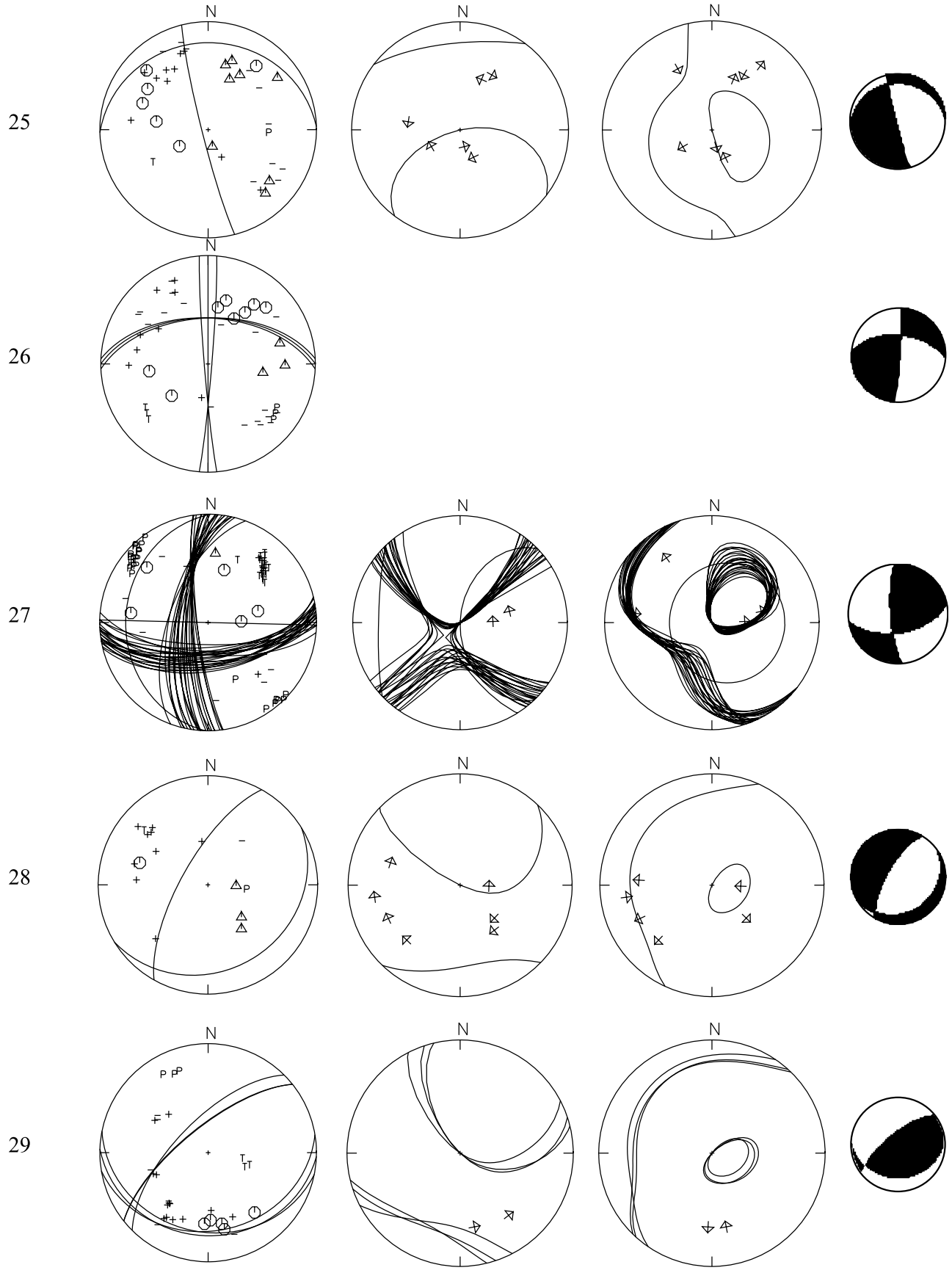

Figure A2. (continued)

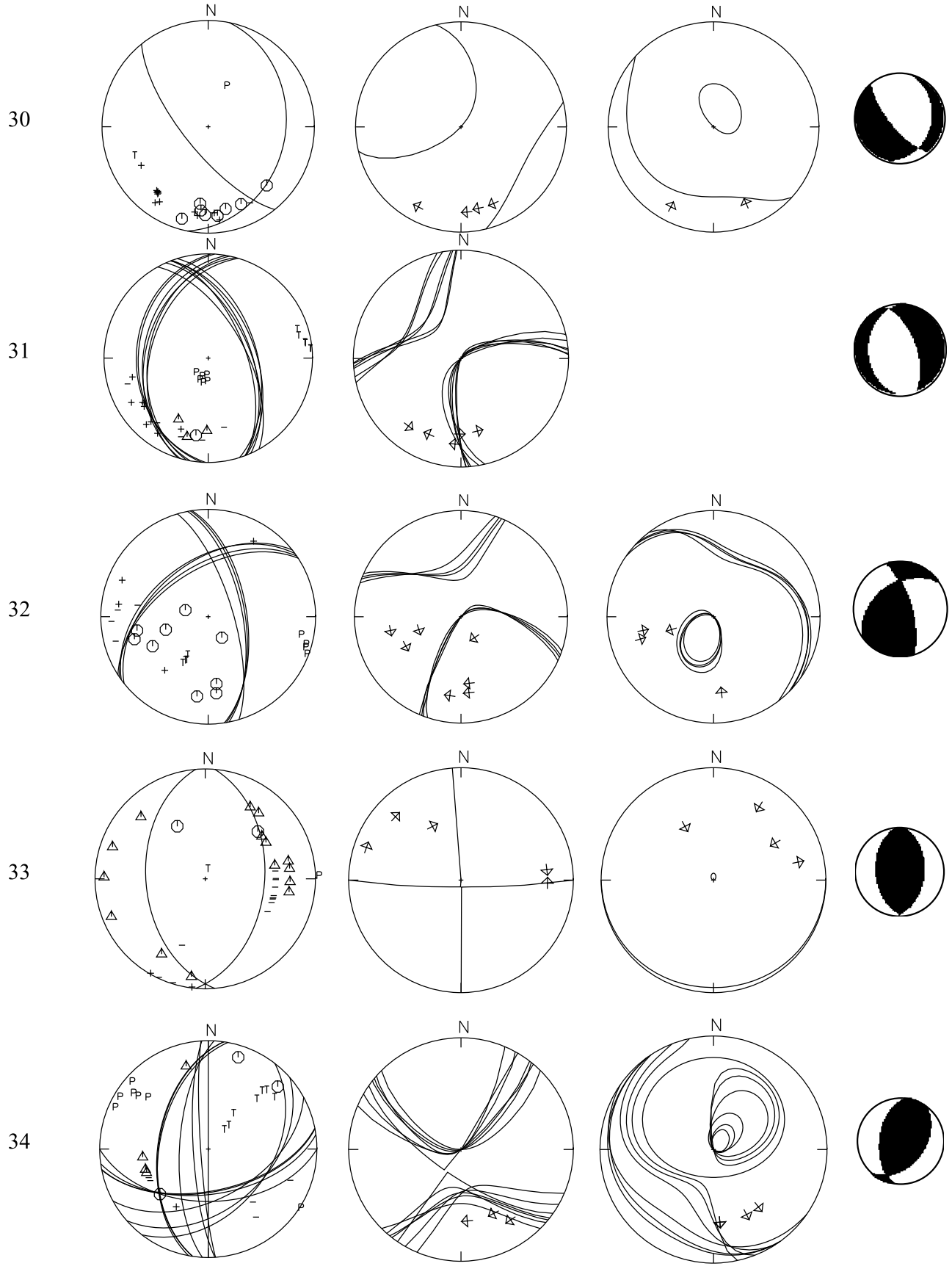

Figure A2. (continued)

35

Figure A2. (continued)

[40] **Acknowledgments.** We thank all the participants to the ESMERALDAS experiment. We are particularly grateful to the Instituto Oceanografico de la Armada and the Instituto Geofisico de la Escuela Politecnica del Ecuador for their help during ESMERALDAS projects and for providing the regional earthquake database. Mario Ruiz is also thanked for his fruitful comments and suggestions. Thank you to Florence Bigot Cormier and Patricia Mothes for improving the English.

References

Agudelo, W. (2005), Imagerie sismique quantitative de la marge convergente d'Equateur-Colombie: Application des méthodes tomographiques aux données de sismique réflexion multitrace et réfraction-réflexion grand-angle des campagnes SISTEUR et SALIERI, thèse de doctorat thesis, 203 pp., Univ. Paris 6 Pierre et Marie Curie, Villefranche-sur-Mer, France.

Agudelo, W., A. Ribodetti, J.-Y. Collot, and S. Operto (2009), Joint inversion of multichannel seismic reflection and wide-angle seismic data: Improved imaging and refined velocity model of the crustal structure of the North Ecuador–South Colombia convergent margin, *J. Geophys. Res.*, *114*, B02306, doi:10.1029/2008JB005690.

Aki, K., and P. G. Richards (1980), *Quantitative Seismology*, 557 pp., Freeman, San Francisco, Calif.

Bassin, C., G. Laske, and G. Masters (2000), The current limits of resolution for surface wave tomography in North America, *Eos Trans. AGU*, *81*, 897.

Beck, S. L., and L. J. Ruff (1984), The rupture process of the great 1979 Colombia earthquake: Evidence for the asperity model, *J. Geophys. Res.*, *89*, 9281–9291, doi:10.1029/JB089iB11p09281.

Benítez, S. (1995), Évolution géodynamique de la province côtière sud-équatorienne au crétacé supérieur—Tertiaire, *Geol. Alp.*, *71*, 3–163.

Bès de Berc, S., J. C. Soula, P. Baby, M. Souris, F. Christophoul, and J. Rosero (2005), Geomorphic evidence of active deformation and uplift in a modern continental wedge-top-foredeep transition: Example of the eastern Ecuadorian Andes, *Tectonophysics*, *399*, 351–380, doi:10.1016/j.tecto.2004.12.030.

Bollinger, L., J. P. Avouac, R. Cattin, and M. R. Pandey (2004), Stress buildup in the Himalaya, *J. Geophys. Res.*, *109*, B11405, doi:10.1029/2003JB002911.

Bondár, I., S. C. Myers, E. R. Engdahl, and E. A. Bergman (2004), Epicentre accuracy based on seismic network criteria, *Geophys. J. Int.*, *156*, 483–496, doi:10.1111/j.1365-246X.2004.02070.x.

Bourdon, E., J.-P. Eissen, M.-A. Gutscher, M. Monzier, M. L. Hall, and J. Cotten (2003), Magmatic response to early aseismic ridge subduction: The Ecuadorian margin case (South America), *Earth Planet. Sci. Lett.*, *205*, 123–138, doi:10.1016/S0012-821X(02)01024-5.

Bryant, J. A., G. M. Yogodzinski, M. L. Hall, J. L. Lewicki, and D. G. Bailey (2006), Geochemical constraints on the origin of volcanic rocks from the Andean northern volcanic zone, Ecuador, *J. Petrol.*, *47*, 1147–1175.

Calahorrano, A., P. Charvis, J.-Y. Collot, F. Sage, and E. R. Flueh (2004), 2D crustal velocity model of subduction in the Gulf of Guayaquil (Ecuador): Reflection and refraction modelling, paper A-05083 presented at 04 Spring Meeting, Eur. Geosci. Union, Nice, France.

Calahorrano, A., V. Sallarès, J.-Y. Collot, F. Sage, and C. R. Ranero (2008), Structure and physical properties of the subduction channel off the Gulf of Guayaquil (Ecuador) from seismic reflection data, *Earth Planet. Sci. Lett.*, *267*, 453–467, doi:10.1016/j.epsl.2007.11.061.

Cantalamessa, G., and C. Di Celma (2004), Origin and chronology of Pleistocene marine terraces of Isla de la Plata and of flat, gently dipping surfaces of the southern coast of Cabo San Lorenzo (Manabi, Ecuador), *J. South Am. Earth Sci.*, *16*, 633–648, doi:10.1016/j.jsames.2003.12.007.

Cediel, F., R. P. Shaw, and C. Càceres (2003), Tectonic assembly of the northern Andean Block, in *The Circum-Gulf of Mexico and the Caribbean: Hydrocarbon Habitats, Basin Formation, and Plate Tectonics*, edited by C. Bartolini, R. T Buffler, and J. F. Blickwede, pp. 815–848, Am. Assoc. Pet. Geol., Tulsa, Okla.

Chapple, W. M., and D. W. Forsyth (1979), Earthquakes and bending of plates at trenches, *J. Geophys. Res.*, *84*, 6729–5749.

Christophoul, F., P. Baby, and C. Davila (2002), Stratigraphic responses to a major tectonic event in a foreland basin: The Ecuadorian Oriente Basin from Eocene to Oligocene times, *Tectonophysics*, *345*, 281–298, doi:10.1016/S0040-1951(01)00217-7.

Collot, J.-Y., P. Charvis, M.-A. Gutsher, and S. Operto (2002), Exploring the Ecuador-Colombia active margin and interplate seismogenic zone, *Eos Trans. AGU*, *83*, 185, doi:10.1029/2002EO000120.

Collot, J.-Y., B. Marcaillou, F. Sage, F. Michaud, W. Agudelo, P. Charvis, D. Graindorge, M.-A. Gutscher, and G. Spence (2004), Are rupture zone limits of great subduction earthquakes controlled by upper plate structures? Evidence from multichannel seismic reflection data acquired across the northern Ecuador–southwest Colombia margin, *J. Geophys. Res.*, *109*, B11103, doi:10.1029/2004JB003060.

Collot, J.-Y., W. Agudelo, A. Ribodetti, and B. Marcaillou (2008), Origin of a crustal splay fault and its relation to the seismogenic zone and underplating at the erosional North Ecuador–South Colombia oceanic margin, *J. Geophys. Res.*, *113*, B12102, doi:10.1029/2008JB005691.

d'Acremont, E., A. Ribodetti, J. Y. Collot, and F. Sage (2005), Margin structure and destabilisation processes on the Colombia-Ecuador margin by 2D quantitative seismic imaging, paper presented at General Assembly, Eur. Geosci. Union, Vienna, 24–29 Apr.

Daly, M. C. (1989), Correlations between Nazca/Farallon plate kinematics and forearc basin evolution in Ecuador, *Tectonics*, *8*, 769–790, doi:10.1029/TC008i004p00769.

Deniaud, Y. (2000), Enregistrement Sédimentaire et Structural de l'Évolution Géodynamique des Andes Equatoriennes au Cours du Néogène: Étude des Bassins d'Avant-Arc et Bilan de Masse, 157 pp., Univ. Joseph Fourier, Grenoble, France.

Dumont, J. F., E. Santana, W. Vilema, K. Pedoja, M. Ordonez, M. Cruz, N. Jimenez, and I. Zambrano (2005), Morphological and microtectonic analysis of Quaternary deformation from Puna and Santa Clara Islands, Gulf of Guayaquil, Ecuador (South America), *Tectonophysics*, *399*, 331–350, doi:10.1016/j.tecto.2004.12.029.

Dziewonski, A. M., T.-A. Chou, and J. H. Woodhouse (1981), Determination of earthquake source parameters from waveform data for studies of global and regional seismicity, *J. Geophys. Res.*, *86*, 2825–2852.

Ego, F., M. Sébrier, A. Lavenu, H. Yepes, and A. Egues (1996), Quaternary state of stress in the northern Andes and the restraining bend model for the Ecuadorian Andes, *Tectonophysics*, *259*, 101–116, doi:10.1016/0040-1951(95)00075-5.

Eguez, A., M. N. Machette, A. Alvarado, H. Yepes, and R. L. Dart (2003), Map of Quaternary faults and folds of Ecuador and its offshore region: International Lithosphere Program Task Group II-2—Major active faults of the world, U.S. Geol. Surv., Denver, Colo.

Engdahl, E. R., and A. Villaseñor (2002), Global seismicity: 1990–1999, in *International Handbook of Earthquakes and Engineering Seismology: Part A*, edited by W. H. K. Lee et al., chap. 41, *Int. Geophys.*, *81*, 665–690, doi:10.1016/S0074-6142(02)80244-3.

Espurt, N., F. Funiciello, J. Martinod, B. Guillaume, V. Regard, C. Faccenna, and S. Brusset (2008), Flat subduction dynamics and deformation of the South American plate: Insights from analog modeling, *Tectonics*, *27*, TC3011, doi:10.1029/2007TC002175.

Fedotov, S. A. (1965), Regularities of the distribution of strong earthquakes in Kamchatka, the Kurile Islands and northeast Japan, *Tr. Inst. Fiz. Zemli. Acad. Nauk. SSSR*, *36*, 66–93.

Gailler, A., P. Charvis, and E. R. Flueh (2007), Segmentation of the Nazca and South American plates along the Ecuador subduction zone from wide angle seismic profiles, *Earth Planet. Sci. Lett.*, *260*, 444–464, doi:10.1016/j.epsl.2007.05.045.

Garcia Cano, L. C. (2009), Imagerie sismique 3D de la zone de subduction à la frontière Colombie-Equateur, Ph.D. thesis, 232 pp., Univ. Nice-Sophia Antipolis, Villefranche-sur-Mer, France.

Garrison, J. M., and J. P. Davidson (2003), Dubious case for slab melting in the northern volcanic zone of the Andes, *Geology*, *31*, 565–568.

Gerbault, M., J. Cembrano, C. Mpodozis, M. Farias, and M. Pardo (2009), Continental margin deformation along the Andean subduction zone: Thermo-mechanical models, *Phys. Earth Planet. Inter.*, *177*, 180–205, doi:10.1016/j.pepi.2009.09.001.

Graindorge, D., A. Calahorrano, P. Charvis, J.-Y. Collot, and N. Bethoux (2004), Deep structures of the Ecuador convergent margin and the Carnegie Ridge, possible consequence on great earthquakes recurrence interval, *Geophys. Res. Lett.*, *31*, L04603, doi:10.1029/2003GL018803.

Guillier, B., J.-L. Chatellain, A. Alvarado, H. Yepes, G. Poupinet, and J.-F. Fels (1996), Lithoscope experiment in northern Ecuador: Preliminary results, paper presented at ISAG 1996, in Andean Geodynamics, edited by M. Gerbault, G. Hérail, and J. Martinod, pp. 55–58, ORSTOM, Saint-Malo, France.

Guillier, B., J.-L. Chatelain, É. Jaillard, H. Yepes, G. Poupinet, and J.-F. Fels (2001), Seismological evidence on the geometry of the orogenic system in central-northern Ecuador (South America), *Geophys. Res. Lett.*, *28*, 3749–3752, doi:10.1029/2001GL013257.

Gutenberg, B., and C. F. Richter (1959), *Seismicity of the Earth*, 310 pp., Princeton Univ. Press, Princeton, N. J.

Gutscher, M.-A., J. Malavieille, S. Lallemand, and J.-Y. Collot (1999), Tectonic segmentation of the North Andean margin: Impact of the Carnegie Ridge collision, *Earth Planet. Sci. Lett.*, *168*, 255–270, doi:10.1016/S0012-821X(99)00060-6.

Gutscher, M.-A., W. Spakman, H. Bijwaard, and E. R. Engdahl (2000), Geodynamics of flat subduction: Seismicity and tomographic constraints from the Andean margin, *Tectonics*, *19*, 814–833, doi:10.1029/1999TC001152.

Hacker, B. R., S. M. Peacock, G. A. Abers, and S. D. Holloway (2003), Subduction factory: 2. Are intermediate-depth earthquakes in subducting slabs linked to metamorphic dehydration reactions?, *J. Geophys. Res.*, *108*(B1), 2030, doi:10.1029/2001JB001129.

Hall, M. L., and C. A. Wood (1985), Volcano-tectonic segmentation of the northern Andes, *Geology*, *13*, 203–207.

Hall, M. L., and H. Yepes (1982), Fallamiento y actividad microsismica en el Valle Interandino, Ecuador: Instituto Panamericano de geografia e historia, *Rev. Geofis.*, *13*, 43–56.

Hardy, N. C. (1991), Tectonic evolution of the easternmost Panama Basin: Some new data and inferences, *J. South Am. Earth Sci.*, *4*, 261–269, doi:10.1016/0895-9811(91)90035-J.

Havskov, J., and L. Ottemöller (1999), SeisAn earthquake analysis software, *Seismol. Res. Lett.*, *70*, 532–534, doi:10.1785/gssrl.70.5.532.

Hello, Y., B. A. Yates, A. Anglade, A. Gailler, and P. Charvis (2006), Hippocampe: A new versatile ocean bottom seismometer, paper presented at General Assembly 2006, Eur. Geosci. Union, Vienna.

Herd, D. G., T. L. Youd, H. Meyer, J. L. Arango, C. W. J. Person, and C. Mendoza (1981), The Great Tumaco, Colombia earthquake of 12 December 1979, *Science*, *211*, 441–445, doi:10.1126/science.211.4481.441.

Jaillard, E., M. Ordoñez, S. Benítez, G. Berrones, N. Jimenez, G. Montenegro, and I. Zambrano (1995), Basin development in an accretionary, oceanic-floored fore-arc setting: Southern coastal Ecuador during late Cretaceous–late Eocene time, in *Petroleum Basins of South America*, edited by A. J. Tankard, R. Suárez, and H. J. Welsink, pp. 615–631, Am. Assoc. Pet. Geol., Tulsa, Okla.

Jaillard, E., S. Benítez, and G. H. Mascle (1997), Les déformations paléogènes de la zone d'avant-arc sud-equatorienne en relation avec l'évolution géodynamique, *Bull. Soc. Geol. Fr.*, *168*, 403–412.

Jordan, T. E., B. L. Isacks, R. W. Allmendinger, J. A. Brewer, V. A. Ramos, and C. J. Ando (1983), Andean tectonics related to geometry of subducted Nazca Plate, *Geol. Soc. Am. Bull.*, *94*, 341–361.

Kanamori, H. (1986), Rupture process of subduction zone earthquakes, *Annu. Rev. Earth Planet. Sci.*, *14*, 293–322, doi:10.1146/annurev.ea.14.050186.001453.

Kanamori, H., and J. W. Given (1981), Use of long-period surface waves for rapid determination of earthquake-source parameters, *Phys. Earth Planet. Inter.*, *27*, 8–31, doi:10.1016/0031-9201(81)90083-2.

Kanamori, H., and K. C. McNally (1982), Variable rupture mode of the subduction zone along the Ecuador-Colombia coast, *Bull. Seismol. Soc. Am.*, *72*, 1241–1253.

Kelleher, J. A. (1972), Rupture zones of large South American earthquakes and some predictions, *J. Geophys. Res.*, *77*, 2087–2103, doi:10.1029/JB077i011p02087.

Kellogg, J. N., and V. Vega (1995), Tectonic development of Panama, Costa Rica, and the Colombian Andes: Constraints from Global Positioning System geodetic studies and gravity, *Spec. Pap. Geol. Soc. Am.*, *295*, 75–90.

Kendrick, E., M. Bevis, R. Smalley, B. Brooks, R. B. Vargas, E. Lauría, and L. P. S. Fortes (2003), The Nazca–South America Euler vector and its rate of change, *J. South Am. Earth Sci.*, *16*, 125–131, doi:10.1016/S0895-9811(03)00028-2.

Kerr, A. C., J. A. Aspden, J. Tarney, and L. F. Pilatasig (2002), The nature and provenance of accreted oceanic terranes in western Ecuador: Geochemical and tectonic constraints, *J. Geol. Soc.*, *159*, 577–594, doi:10.1144/0016-764901-151.

Lahr, J. C. (1999), HYPOELLIPSE: A computer program for determining local earthquake hypocentral parameter, magnitude, and first-motion pattern, *U.S. Geol. Surv. Open File Rep., 99-23*, 116 pp.

Lay, T., and H. Kanamori (1981), An asperity model of great earthquake sequences, in *Earthquake Prediction: An International Review*, *Maurice Ewing Ser.*, vol. 4, edited by D. W. Simpson and P. G. Richards, pp. 579–592, AGU, Washington, D. C.

Lay, T., H. Kanamori, and L. Ruff (1982), The asperity model and the nature of large subduction zone earthquakes, *Earthquake Predict. Res.*, *1*, 3–71.

Lonsdale, P. (1978), Ecuadorian subduction system, *AAPG Bull.*, *62*, 2454–2477.

Luzieux, L. D. A., F. Heller, R. Spikings, C. F. Vallejo, and W. Winkler (2006), Origin and Cretaceous tectonic history of the coastal Ecuadorian forearc between 1°N and 3°S: Paleomagnetic, radiometric and fossil evidence, *Earth Planet. Sci. Lett.*, *249*, 400–414, doi:10.1016/j.epsl.2006.07.008.

Marcaillou, B., G. Spence, K. Wang, J.-Y. Collot, and A. Ribodetti (2008), Thermal segmentation along the N. Ecuador–S. Colombia margin (1–4°N): Prominent influence of sedimentation rate in the trench, *Earth Planet. Sci. Lett.*, *272*, 296–308, doi:10.1016/j.epsl.2008.04.049.

Mendoza, C., and J. W. Dewey (1984), Seismicity associated with the great Colombia-Ecuador earthquakes of 1942, 1958 and 1979: Implications for barrier models of earthquake rupture, *Bull. Seismol. Soc. Am.*, *74*, 577–593.

Michaud, F., J.-Y. Collot, A. Alvarado, E. López, INOCAR, and República de Ecuador (2006), Batimetría y relieve continental, *IOA-CVM-02-Post, INOCAR*, Guayaquil, Ecuador.

Michaud, F., C. Witt, and J. Y. Royer (2009), Influence of the subduction of the Carnegie volcanic ridge on Ecuadorian geology: Reality and fiction, *Mem. Geol. Soc. Am.*, *204*.

Mogi, K. (1977), Dilatancy of rocks under general triaxial stress states with special references to earthquake precursors, *J. Phys. Earth*, *25*, S203–S217.

Mogi, K. (1985), *Earthquake Prediction*, 355 pp., Academic, New York.

Monzier, M., C. Robin, C. Hall, M. L. Cotten, J. Mothes, P. Eissen, and J. P. Samaniego (1997), Les adakites d'Equateur: Modèle préliminaire, *C. R. Acad. Sci.*, *324*.

Nakamura, M. (2002), Determination of focal mechanism solution using initial motion polarity of P and S waves, *Phys. Earth Planet. Inter.*, *130*, 17–29, doi:10.1016/S0031-9201(01)00306-5.

Nishenko, S. P. (1991), Circum-Pacific seismic potential 1989–1999, *Pure Appl. Geophys.*, *135*, 169–259, doi:10.1007/BF00880240.

Nocquet, J. M., P. Mothes, and A. Alvarado (2009), Geodesia, geodinamica y ciclo sismico en Ecuador, in *Geologia y Geofisica Marina y Terrestre del Ecuador*, edited by J. Y. Collot et al., pp. 83–95, INOCAR, Guayaquil, Ecuador.

Ocola, L. C., L. T. Aldrich, J. F. Gettrust, R. P. Meyer, and J. E. Ramirez (1975), Project NARINO 1: Crustal structure under southern Colombian–northern Ecuador Andes from seismic refraction data, *Bull. Seismol. Soc. Am.*, *65*, 1681–1695.

Pardo, M., D. Comte, and T. Monfret (2002), Seismotectonic and stress distribution in the central Chile subduction zone, *J. South Am. Earth Sci.*, *15*, 11–22, doi:10.1016/S0895-9811(02)00003-2.

Pedoja, K., J. F. Dumont, M. Lamothe, L. Ortlieb, J. Y. Collot, B. Ghaleb, M. Auclair, V. Alvarez, and B. Labrousse (2006a), Plio-Quaternary uplift of the Manta Peninsula and La Plata Island and the subduction of the Car-

negie Ridge, central coast of Ecuador, *J. South Am. Earth Sci.*, *22*, 1–21, doi:10.1016/j.jsames.2006.08.003.

Pedoja, K., L. Ortlieb, J. F. Dumont, M. Lamothe, B. Ghaleb, M. Auclair, and B. Labrousse (2006b), Quaternary coastal uplift along the Talara Arc (Ecuador, northern Peru) from new marine terrace data, *Mar. Geol.*, *228*, 73–91, doi:10.1016/j.margeo.2006.01.004.

Pennington, W. D. (1981), Subduction of the eastern Panama Basin and seismotectonics of northwestern South America, *J. Geophys. Res.*, *86*, 10,753–10,770, doi:10.1029/JB086iB11p10753.

Pontoise, B., and T. Monfret (2004), Shallow seismogenic zone detected from an offshore-onshore temporary seismic network in the Esmeraldas area (northern Ecuador), *Geochem. Geophys. Geosyst.*, *5*, Q02009, doi:10.1029/2003GC000561.

Ramos, V. A., and A. Folguera (2009), Andean flat-slab subduction through time, *Geol. Soc. Spec. Publ.*, *327*, 31–54.

Ranero, C. R., A. Villaseñor, J. Phipps Morgan, and W. Weinrebe (2005), Relationship between bend-faulting at trenches and intermediate-depth seismicity, *Geochem. Geophys. Geosyst.*, *6*, Q12002, doi:10.1029/2005GC000997.

Ratzov, G., J. Y. Collot, M. Sosson, and S. Migeon (2010), Mass-transport deposits in the northern Ecuador subduction trench: Result of frontal erosion over multiple seismic cycles, *Earth Planet. Sci. Lett.*, *296*, 89–102, doi:10.1016/j.epsl.2010.04.048.

Regnier, M., J.-L. Chatelain, R. J. Smalley, J. M. Chiu, B. L. Isacks, and M. Araujo (1992), Seismotectonics of the sierra pie de Palo, a basement block uplift in the Andean foreland of Argentina, *Bull. Seismol. Soc. Am.*, *82*, 2549–2571.

Reid, H. F. (1910), The mechanism of the earthquake, in *The California Earthquake of April 18, 1906: Report of the State Earthquake Investigation Commission*, 192 pp., Carnegie Inst., Washington, D. C.

Reynaud, C., E. Jaillard, H. Lapierre, M. Mamberti, and G. H. Mascle (1999), Oceanic plateau and island arcs of southwestern Ecuador: Their place in the geodynamic evolution of northwestern South America, *Tectonophysics*, *307*, 235–254, doi:10.1016/S0040-1951(99)00099-2.

Sallarès, V., and P. Charvis (2003), Crustal thickness constraints on the geodynamic evolution of the Galapagos Volcanic Province, *Earth Planet. Sci. Lett.*, *214*, 545–559, doi:10.1016/S0012-821X(03)00373-X.

Sallarès, V., P. Charvis, E. R. Flueh, J. Bialas, and the SALIERI Scientific Party (2005), Seismic structure of the Carnegie ridge and the nature of the Galápagos hotspot, *Geophys. J. Int.*, *161*, 763–788, doi:10.1111/j.1365-246X.2005.02592.x.

Samaniego, P., H. Martin, C. Robin, and M. Monzier (2002), Transition from calc-alkalic to adakitic magmatism at Cayambe volcano, Ecuador: Insights into slab melts and mantle wedge interactions, *Geology*, *30*, 967–970.

Samaniego, P., H. Martin, M. Monzier, C. Robin, M. Fornari, J.-P. Eissen, and J. Cotten (2005), Temporal evolution of magmatism in the northern volcanic zone of the Andes: The geology and petrology of Cayambe Volcanic Complex (Ecuador), *J. Petrol.*, *46*, 2225–2252.

Scholz, C. H. (1988), The brittle-ductile transition and the depth of seismic faulting, *Geol. Rundsch.*, *77*, 319–328, doi:10.1007/BF01848693.

Scholz, C. H. (1990), *The Mechanics of Earthquakes and Faulting*, 439 pp., Cambridge Univ. Press, New York.

Segovia, M. (2001), El sismo de Bahía del 4 de agosto de 1998: Caracterización del mecanismo de ruptura y análisis de la sismicidad en la zona costera, thesis, Escuela Politec. Nac., Quito.

Snoke, J. A., J. W. Munsey, A. G. Teague, and G. A. Bolliger (1984), A program for focal mechanism determination by combined use of polarity and SV-P amplitude ratio data, *Earthquake Notes*, *55*, 15.

Stauder, W. (1975), Subduction of the Nazca plate under Peru as evidenced by focal mechanisms and by seismicity, *J. Geophys. Res.*, *80*, 1053–1064, doi:10.1029/JB080i008p01053.

Stein, R. S., and G. Ekstrom (1992), Seismicity and geometry of a 110-km-long blind thrust fault: 2. Synthesis of the 1982–1985 California earthquake sequence, *J. Geophys. Res.*, *97*, 4865–4883, doi:10.1029/91JB02847.

Swenson, J. L., and S. L. Beck (1996), Historical 1942 Ecuador and 1942 Peru subduction earthquakes and earthquake cycles along Colombia-Ecuador and Peru subduction segments, *Pure Appl. Geophys.*, *146*, 67–101, doi:10.1007/BF00876670.

Tichelaar, B. W., and L. J. Ruff (1993), Depth of seismic coupling among subduction zones, *J. Geophys. Res.*, *98*, 2017–2037, doi:10.1029/92JB02045.

Trenkamp, R., J. N. Kellogg, J. T. Freymueller, and H. P. Mora (2002), Wide plate margin deformation, southern Central America and northwestern South America, CASA GPS observations, *J. South Am. Earth Sci.*, *15*, 157–171, doi:10.1016/S0895-9811(02)00018-4.

Vaca, S., M. Régnier, N. Béthoux, V. Alvarez, and B. Pontoise (2009), Sismicidad de la región de Manta: Enjambre sísmico de Manta-2005, in *Geologia y Geofisica Marina y Terrestre del Ecuador Desde la Costa Continental Hasta las Islas Gapapagos*, edited by J. Y. Collot et al., pp. 151–166, INOCAR, Guayaquil, Ecuador.

Wadati, K. (1933), On travel time of earthquake waves, Part II, *Geophys. Mag.*, *7*, 101–111.

Wagner, L. S., S. Beck, and G. Zandt (2005), Upper mantle structure in the south central Chilean subduction zone (30° to 36°S), *J. Geophys. Res.*, *110*, B01308, doi:10.1029/2004JB003238.

Warren, L. M., M. A. Langstaff, and P. G. Silver (2008), Fault plane orientations of intermediate-depth earthquakes in the Middle America Trench, *J. Geophys. Res.*, *113*, B01304, doi:10.1029/2007JB005028.

White, S. C., R. Trenkamp, and J. N. Kellogg (2003), Recent crustal deformation and the earthquake cycle along the Ecuador-Colombia subduction zone, *Earth Planet. Sci. Lett.*, *216*, 231–242, doi:10.1016/S0012-821X(03)00535-1.

Winkler, W., D. Villagomez, R. Spikings, P. Abegglen, S. Tobler, and A. Eguez (2005), The Chota basin and its significance for the inception and tectonic setting of the inter-Andean depression in Ecuador, *J. South Am. Earth Sci.*, *19*, 5–19, doi:10.1016/j.jsames.2004.06.006.

Witt, C., and J. Bourgois (2010), Forearc basin formation in the tectonic wake of a collision-driven, coastwise migrating crustal block: The example of the North Andean block and the extensional Gulf of Guayaquil-Tumbes basin (Ecuador-Peru border area), *Geol. Soc. Am. Bull.*, *122*, 89–108, doi:10.1130/B26386.1.

Witt, C., J. Bourgois, F. Michaud, M. Ordoñez, N. Jiménez, and M. Sosson (2006), Development of the Gulf of Guayaquil (Ecuador) during the Quaternary as an effect of the North Andean block tectonic escape, *Tectonics*, *25*, TC3017, doi:10.1029/2004TC001723.

N. Béthoux and K. Manchuel, UMR Geoazur, University of Nice–Sophia Antipolis, Port de la Darse, BP 48, F-06235 Villefranche-sur-Mer, France. (nbethoux@geoazur.obs-vlfr.fr; manchuel@geoazur.obs-vlfr.fr)

J. Díaz, Departamento Geofisica i Tectonica, Institut de Ciències de la Terra "Jaume Almera" IJA-CSIC, Lluis Solé i Sabaris s/n, E-08028 Barcelona, Spain. (jdiaz@ija.csic.es)

Y. Font, UMR Geoazur, University of Nice–Sophia Antipolis, IRD, Port de la Darse, BP 48, F-06235 Villefranche-sur-Mer, France. (font@geoazur.obs-vlfr.fr)

M. Régnier, UMR Geoazur, University of Nice–Sophia Antipolis, IRD, 250 Rue Albert Einstein, Sophia-Antipolis, F-06560 Valbonne, France. (regnier@geoazur.unice.fr)

V. Sallarès, Unidad de Tecnología Marina, Consejo Superior de Investigaciones Científicas, Passeig Maritim de la Barceloneta, 37-49, E-08003 Barcelona, Spain. (vsallares@cmima.csic.es)

H. Yepes, Instituto Geofisico de la Escuela Politecnica Nacional, Ladrón de Guevara e11-253, Apartado 2759, Quito, Ecuador. (hyepes@igepn.edu.ec)